Contribution of Tropical Cyclones to Global Very Deep Convection

HAIYAN JIANG AND CHENG TAO

Department of Earth and Environment, Florida International University, Miami, Florida

(Manuscript received 1 February 2013, in final form 21 February 2014)

ABSTRACT

Based on the 12-yr (1998–2009) Tropical Rainfall Measuring Mission (TRMM) precipitation feature (PF) database, both radar and infrared (IR) observations from TRMM are used to quantify the contribution of tropical cyclones (TCs) to very deep convection (VDC) in the tropics and to compare TRMM-derived properties of VDC in TCs and non-TCs. Using a radar-based definition, it is found that the contribution of TCs to total VDC in the tropics is not much higher than the contribution of TCs to total PFs. However, the area-based contribution of TCs to overshooting convection defined by IR is 13.3%, which is much higher than the 3.2% contribution of TCs to total PFs. This helps explain the contradictory results between previous radar-based and IR-based studies and indicates that TCs only contribute disproportionately large amount of overshooting convection containing mainly small ice particles that are barely detected by the TRMM radar. VDC in non-TCs over land has the highest maximum 30- and 40-dBZ height and the strongest ice-scattering signature derived from microwave 85- and 37-GHz observations, while VDC in TCs has the coldest minimum IR brightness temperature and largest overshooting distance and area. This suggests that convection is much more intense in non-TCs over land but is much deeper or colder in TCs. It is found that VDC in TCs usually has smaller environmental shear but larger total precipitable water and convective available potential energy than those in non-TCs. These findings offer evidence that TCs may contribute disproportionately to troposphere-to-stratosphere heat and moisture exchange.

1. Introduction

The transition of mass and energy between the upper tropical troposphere and lower stratosphere is of great importance on the maintenance of the general circulation. Newell and Gould-Stewart (1981) termed the restricted region of entry of troposphere air into the stratosphere as the stratosphere fountain and found that it is related to areas with very strong convection. Other studies have further suggested that one of the most essential agents for heat and moisture transportation is the existence of deep tropical cumulonimbus clouds (Riehl and Malkus 1958; Simpson 1990; Holton et al. 1995; Dessler 2002). When these tall cumulonimbus clouds reach or penetrate the tropopause, they are usually referred as ''hot towers'' or overshooting convection. Part of the overshooting convection in the tropics and subtropics occurs in tropical cyclones (TCs). Ebert and Holland (1992) documented a case of overshooting convection in Tropical Cyclone Hilda (1990) with minimum infrared (IR) brightness temperature of about 173 K, which was the coldest cloud-top temperature ever recorded.

An interesting question in TC research is: what role do TCs play in the heat and moisture transportation between the troposphere and stratosphere? Because of the large size of the moist ascent regions in TCs, it is reasonable to speculate that deep convection in TCs may be subject to less entrainment drying as those in other mesoscale systems, therefore having a higher percentage of convection that is very deep and penetrates a level near or reaching the tropopause. Using one year (1999) of the Tropical Rainfall Measuring Mission (TRMM) satellite radar data, Cairo et al. (2008) roughly estimated the fraction of TC-related convection that is penetrating 14 km, a level usually considered as a good proxy for the lower edge of the tropical tropopause layer (TTL; Sherwood and Dessler 2001). This fraction was 3.5%, close to the 1.2%–1.8% value obtained by Alcala and Dessler (2002) for the overall convection in the tropics using the 4 months of TRMM radar data. By using a much longer term (11 yr) of TRMM radar observations, Tao and Jiang (2013) found that the fraction of

Corresponding author address: Dr. Haiyan Jiang, Department of Earth and Environment, Florida International University, 11200 SW 8th St., PC-342B, Miami, FL 33199.
E-mail: haiyan.jiang@fiu.edu

DOI: 10.1175/JCLI-D-13-00085.1

precipitation features (PFs; defined as at least four adjacent pixels with near-surface rain rate greater than zero) in TCs that have 20-dBZ radar echo penetrate 14 km was 1.6%, a value close to the 1.4% value obtained by Liu and Zipser (2005) for all PFs in the tropics using 5-yr TRMM radar data. These TRMM radar-based studies seem to indicate that TCs are not a preferred location for TTL-penetrating convection. However, all these studies used the TRMM data from different periods of time, which may introduce uncertainties when drawing conclusions by comparing their results. In addition, TCs and non-TCs are not compared in a same study: that is, Cairo et al. (2008) and Tao and Jiang (2013) only studied TCs, while Alcala and Dessler (2002) and Liu and Zipser (2005) only studied the overall convection in the tropics.

Using 23 years of IR brightness temperatures from the International Satellite Cloud Climatology Project (ISCCP), Romps and Kuang (2009) defined overshooting convection as convection with cloud-top temperatures below the monthly averaged tropopause temperature. They analyzed both TCs and non-TCs and evaluated the contributions of TCs to convection that penetrate a various range of levels from cloud-top temperature 40 K warmer than the tropopause temperature to 15 K colder than that. They found that TCs account for only 7% of the deep convection (cloud-top temperature 40 K warmer than the tropopause) in the tropics but 15% of the overshooting convection (cloud-top temperature colder than the tropopause temperature). This suggested that TCs contribute a disproportionately large amount of convection reaching the stratosphere. However, comparing with radar-based studies, one potential problem with using IR temperature alone is that cirrus clouds might be included as convection.

This study will take a different approach. The TRMM satellite does not only have a precipitation radar (PR) but also a Visible and Infrared Scanner (VIRS). Both radar and IR observations in the same platform will be used to investigate the contribution of TCs to very deep convection in the tropics and to compare radar-derived and IR-derived properties of very deep convection in TCs and non-TCs. Two types of very deep convection will be defined. The first one will be PR based, defined as 20-dBZ radar echo penetrating 14 km. The second one will be IR based, defined as IR cloud-top brightness temperature colder than the tropopause temperature (see section 2b for details). To avoid semantic confusions, in the following text, both types will be referred to as very deep convection in general, while ''overshooting convection'' will be reserved for the second type only. However, the word overshooting will be used for both types when referring to overshooting properties, which include overshooting distance, area, volume, and ice mass by following Liu and Zipser (2005)'s definitions (see section 2c for details). In overshooting properties, ''overshooting'' means overshooting 14 km for the PR-based very deep convection definition and overshooting the tropopause for IR-based definition. This study is confined within the global tropics between 36°S and 36°N, which are the TRMM observation boundaries.

One obvious reason of having two definitions of very deep convection using data from the same platform and same time period is to avoid or be able to clarify potential uncertainties that previous PR-only and IR-only studies had. More importantly, various instruments respond to deep convections in different ways. Cloud-top brightness temperatures from the VIRS IR observations provide a reliable measure of cloud coverage with a 3-km horizontal resolution (Kummerow et al. 1998), while PR gives observations of vertical profiles of radar reflectivity with a high vertical resolution (~250 m) and direct indications of the intensity of convection. Liu et al. (2007) quantified the relationship between PR-observed and IR-observed convective properties in tropical deep convection. Their results were helpful to explain the discrepancy between IR- and PR-retrieved rainfall. However, there is no documented study, at least to the authors' current knowledge, to compare radar-observed and IR-observed very deep convection in TCs. It is hoped that this study will fill in the gap and produce results that will feedback on the global precipitation studies. Another motivation of this study is to provide a geographical distribution of very deep convection in TCs and non-TCs. This distribution can be used to evaluate the simulation output of global atmospheric models.

There are two main goals of this study: 1) to quantify the contribution of TCs to global very deep convection in the tropics and 2) to compare the overshooting properties and convective proxies for very deep convection in TCs and non-TCs. The key questions to be addressed are the following: 1) What is the fraction of global very deep convection that are associated with TCs? 2) Does very deep convection in TCs have a higher than average chance to reach the lower stratosphere? 3) Does very deep convection in TCs have greater overshooting properties and stronger convective intensity compared with its counterparts in over-land and over-ocean non-TCs? 4) What kind of environmental conditions might be responsible for the differences, if any, between properties of very deep convection in TCs and non-TCs? In section 2, the data and methodology used in this study are described. The main results are presented in sections 3 and 4, and conclusions are given in section 5. A list of acronyms and abbreviations are shown in the appendix.

2. Data and methodology

a. Florida International University and University of Utah TRMM Tropical Cyclone PF database

This study utilizes 12-yr (January 1998–December 2009) TRMM satellite data from the University of Utah (UU) TRMM PF database (Nesbitt et al. 2000; Liu et al. 2008), which is generated by grouping continuous pixels satisfying certain criteria into a single entity (e.g., a PF). The database contains nearly 30 million PFs observed by TRMM during the 12-yr study period. There are three levels of data in the TRMM PF database (Liu et al. 2008). Parameters in level-1 of this database are collocated pixel-by-pixel observations and retrievals from TRMM Microwave Imager (TMI), PR, VIRS, and Lightning Imaging System (LIS). All TMI, VIRS, and LIS observations are collocated with the PR data at the PR's pixel size of 5.0 km × 5.0 km (4.3 km × 4.3 km before the TRMM orbital boost in August 2001). Because both VIRS and PR scan through nadir, the brightness temperatures from VIRS at each PR pixel are calculated from radiances at the nearest-neighbor VIRS pixel (Liu et al. 2008). The original VIRS pixel size is 2.4 km × 2.4 km (2.2 km × 2.2 km before boost). Level-2 data of the TRMM PF database consist of statistics-based parameters for each identified feature, such as maximum heights of 20-, 30-, 40-dBZ radar echo (called maximum $Z_{20\mathrm{dB}Z}$, $Z_{30\mathrm{dB}Z}$, and $Z_{40\mathrm{dB}Z}$, respectively); minimum IR 10.8-μm brightness temperature (T_{B11}); minimum 37- and 85-GHz polarization corrected brightness temperatures (PCT; Spencer et al. 1989), etc. Currently, this comprehensive database contains 13 different PF definitions according to various grouping criteria [for a detailed description of the UU TRMM PF database, see Liu et al. (2008)]. In this study, a PF is defined with TRMM PR rainfall product 2A25 (Iguchi et al. 2000) near-surface rain rate greater than zero. To remove small features and include only convective features, each PF selected for this study must have total PR 2A25 raining area $\geq$1000 km^2 and at least one pixel with 85-GHz PCT $\leq$225 K. According to Mohr and Zipser (1996), 85-GHz PCT $\leq$225 K suggests that the rain is convective with a rain rate of at least 10–12 mm h^{-1}. The environmental sounding for each PF is obtained by interpolation from the 6-hourly 1.5° × 1.5° resolution European Centre for Medium-Range Weather Forecasts Interim Re-Analysis (ERA-Interim; Simmons et al. 2006).

To separate PFs associated with TCs and non-TCs, the Florida International University (FIU) and UU TRMM tropical cyclone precipitation feature (TCPF) database (Jiang et al. 2011) is used. In this TCPF database, a TCPF is identified when the distance between TC center and the TRMM PF center is within 500 km, a distance that is commonly used in previous studies to separate TC and non-TC rains (Frank 1976; Lonfat et al. 2004). The best-track data are obtained from National Hurricane Center (NHC) hurricane database (HURDAT; Jarvinen et al. 1984) for the Atlantic and eastern central Pacific basins and from the Joint Typhoon Warning Center (JTWC; http://www.usno.navy.mil/JTWC/) for all the other TC-prone basins. Only TCs that reached tropical storm intensity level or above (maximum wind speed $\geq$34 kt; 1 kt $\approx$ 0.51 m s^{-1}) are included in the TCPF database. Besides existing TRMM-observed properties in the UU TRMM PF database, a series of storm-related parameters are calculated and linearly interpolated into TRMM observation time. For example, land/ocean flag of TC center, storm 12-, 24-, 36-, and 48-h future intensity changes, etc. TCPFs are subjectively classified into three subregions: that is, inner core (IC), inner rainband (IB), and outer rainband (OB) by Jiang et al. (2013) based on convective structure, such as the horizontal fields of radar reflectivity and passive microwave ice scattering. TCPFs are also divided into six TC-prone basins following Jiang and Zipser (2010), which include North Atlantic (ATL), east-central Pacific (EPA), northwest Pacific (NWP), north Indian Ocean (NIO), south Indian Ocean (SIO), and South Pacific (SPA). After separating TCPFs from non-TCPFs, non-TCPFs are further separated into over land and over ocean categories based on the location of the PF center. It should be noted that more than 90% of the TCPFs in this study are over ocean.

b. Definition of very deep convection

As mentioned in the introduction, very deep convection in this study will be defined from two different perspectives by using the TRMM PR and VIRS observations, respectively. Using PR reflectivity profiles, PFs with the maximum $Z_{20\mathrm{dB}Z} \geq$ 14 km are defined as PR-based very deep convection. Because of the sixth-power dependence of radar reflectivity on particle size, 20-dBZ echoes are considerably stronger than anything observed in cirrus clouds. The definition essentially assures that there are large, precipitation-sized particles present at 14-km altitude, which is an evidence of deep convective updrafts (Liu et al. 2007). Therefore, in the following text, the PR-based very deep convection PFs are referred to as deep convective updrafts (DCUs). It is noted that the tropical tropopause is usually located at the 16–17-km layer (Liu and Zipser 2005; Tao and Jiang 2013), a level much higher than the 14-km reference height used here. There are two reasons that 14 km is selected: 1) PR detects more readily the larger particles. Therefore the sample size of very deep convection decreases dramatically when using higher reference levels. Previous studies using PR to define overshooting

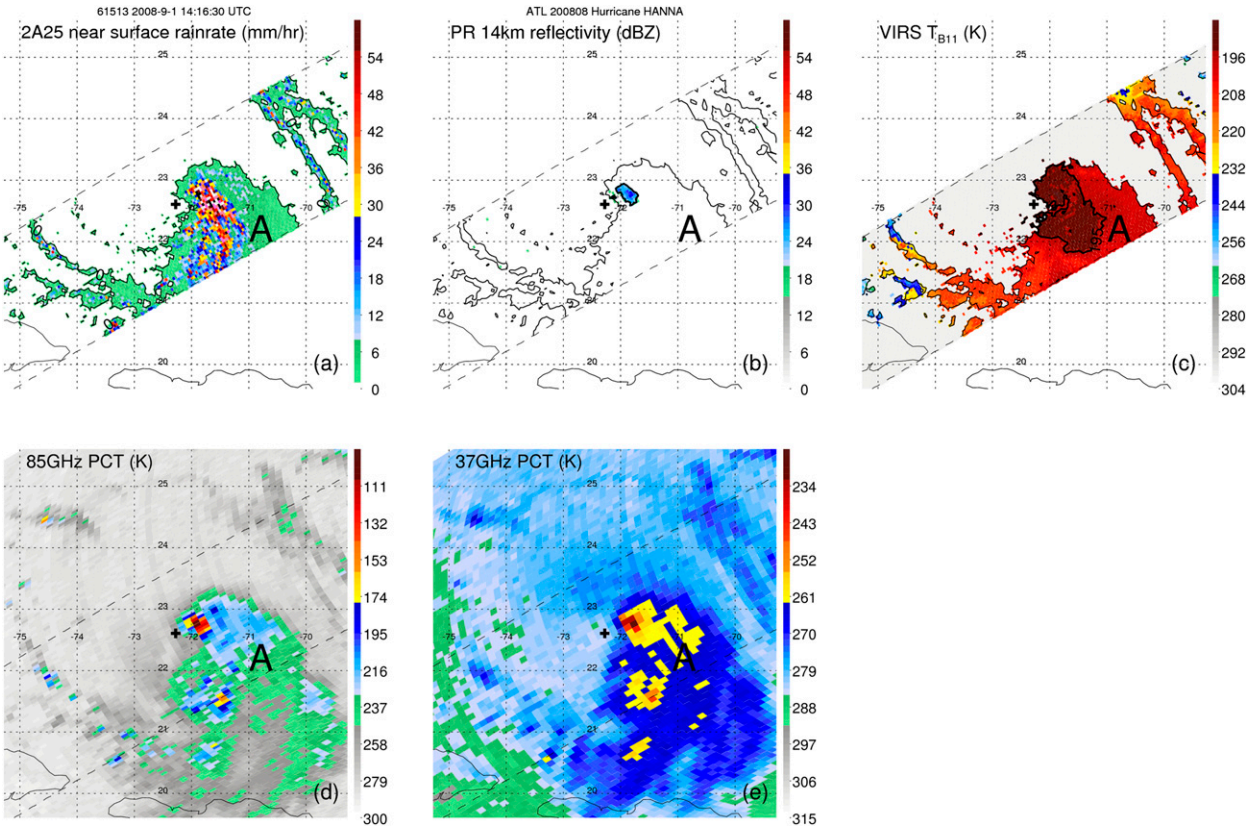

FIG. 1. Examples of (a) PR 2A25 near-surface rain rate (mm h^{-1}), (b) PR reflectivity at 14 km (dBZ), (c) VIRS T_{B11} (K), (d) TMI 85-GHz PCT (K), and (e) TMI 37-GHz PCT (K) from Hurricane Hanna TRMM orbit 61513, at 1416 UTC 1 Sep 2008. The cross at the center of (a)–(e) is the storm center location. The dashed line in each panel is the edge of the PR swath. The thin black contour in (a)–(c) outlines the area with PR 2A25 near-surface rain rate >0. The raining area enclosed in this contour is a PF (demoted as "A" in the figure) satisfying the criteria of PR 2A25 raining area greater than 1000 km^2 and minimum 85-GHz PCT lower than 225 K (please see text for details). The thick black contour in (b) outlines the area with 14-km reflectivity ≥20 dBZ. The thick black contour in (c) outlines the area with $T_{B11} \le T_{trop}$ (T_{trop} = 195 K in this case). Feature A is an example of both DCU and CCT in TCs defined in this study.

convection or "hot towers" all leaned to use 14 km as the reference height (Alcala and Dessler 2002; Liu and Zipser 2005; Cairo et al. 2008; Tao and Jiang 2013). 2) The base of the TTL, which is also known as the level of zero net radiative heating (Sherwood and Dessler 2001), is around 14 km. Several studies suggested that TC-related convection penetrating into the TTL could play an important role in the moisture transportation between troposphere and stratosphere. The PR's minimum detectable signal is approximately 18 dBZ, which varies before and after the boost of the TRMM satellite orbit in August 2001. Here 20 dBZ is arbitrarily chosen for keeping a constant lower limit of PR reflectivity by following Liu and Zipser (2005).

Using the VIRS data, PFs with minimum T_{B11} colder than the tropopause temperature are defined as IR-based very deep convection. The tropopause temperature for each PF is obtained by interpolation from the 6-hourly 1.5° × 1.5° resolution ERA-Interim data. The tropopause is defined as the cold point tropopause. Since the IR brightness temperature is just an indicator of how cold the cloud top is, the IR-based very deep convection PFs are referred to as extremely cold cloud tops (CCTs) in the following text. The CCT definition is very similar to the overshooting convection definition by Romps and Kuang (2009), except that, in the CCT definition, cirrus or cold nonraining anvil clouds are excluded because CCTs are the extreme cases of PFs and the PF definition used in this study requires nonzero surface rain and at least one convective pixel with 85-GHz PCT colder than 225 K. Figure 1 shows an example of a PF in a TRMM overpass of Hurricane Hanna (2008). In this case, the PF satisfies the definitions of both DCU and CCT.

An important question regarding to the DCU and CCT definitions is how these two types of very deep convection are related to each other. Using all DCUs and CCTs identified from the 12-yr TRMM data, Fig. 2 shows the scatterplots of maximum Z_{20dBZ} versus minimum T_{B11}

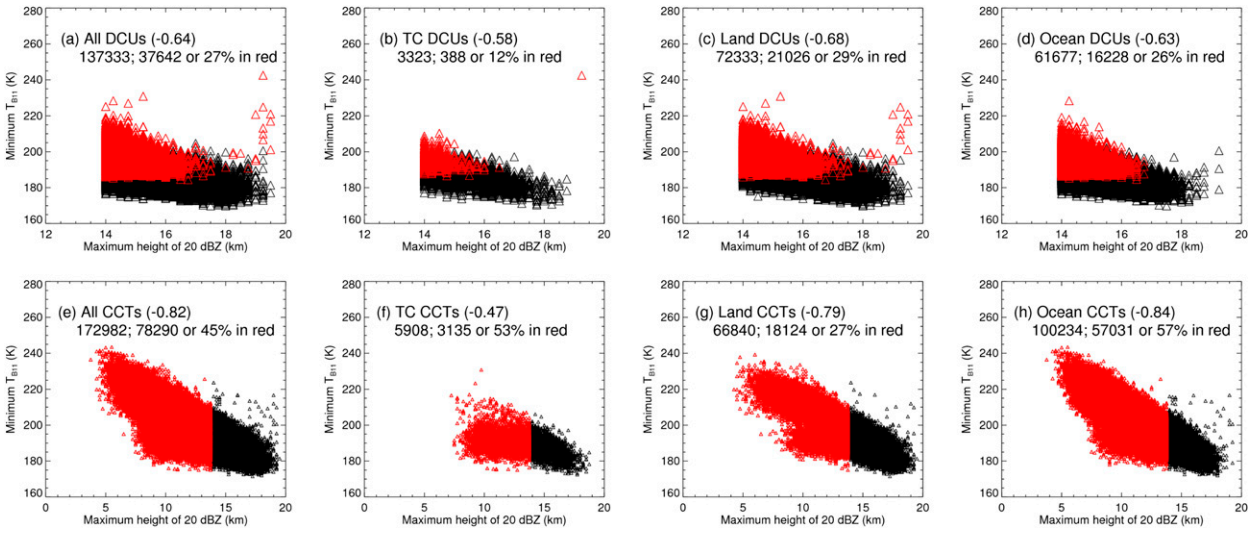

FIG. 2. Scatterplots of maximum 20-dBZ echo height (km) vs minimum T_{B11} (K) for (a) all DCUs, (b) TC DCUs, (c) land DCUs, (d) ocean DCUs, (e) all CCTs, (f) TC CCTs, (g) land CCTs, and (h) ocean CCTs. (top) DCUs that are not CCTs and (bottom) CCTs that are not DCUs are shown in red in each panel. Correlation coefficients between maximum 20-dBZ echo height and minimum T_{B11}, sample size, and samples and percentage in red are also indicated in each panel.

for all DCUs, DCUs in TCs (TC DCUs), DCUs in non-TCs over land (land DCUs) and over ocean (ocean DCUs), all CCTs, CCTs in TCs (TC CCTs), and CCTs in non-TCs over land (land CCTs) and over ocean (ocean CCTs). There are more overshooting cold cloud tops than deep convective updrafts in each category, except that there are slightly more land DCUs than land CCTs. DCUs that are not CCTs and CCTs that are not DCUs are indicated in red. It is clear that the PR-based and IR-based very deep convection is not the same phenomenon, although a generally good correlation is seen between the maximum $Z_{20\mathrm{dB}Z}$ and minimum T_{B11} for all categories. Overall, 27% of DCUs have cloud tops warmer than the tropopause temperature, while a larger percentage (45%) of CCTs have maximum $Z_{20\mathrm{dB}Z}$ lower than 14 km. A much higher fraction (26%–29%) of non-TC DCUs has cloud-top temperature warmer than tropopause than that of TC DCUs (12%). On the other hand, a much higher percentage of ocean and TC CCTs (53%–57%) has maximum $Z_{20\mathrm{dB}Z}$ lower than 14 km than that of land CCTs (27%). This seems to indicate that TC DCUs are easier to generate very small ice particles that can overshoot the tropopause than non-TC DCUs, while land CCTs are easier to have very intense convective updrafts to lift large, precipitation-size particles to 14-km level or above than oceanic and TC (note that more than 90% TCPFs are over ocean) CCTs. The correlation coefficient for all DCUs is lower than that for all CCTs mainly because the sample size of CCTs is larger. The correlation coefficients among TC, land, and ocean categories for DCUs are similar. Interestingly, the correlation coefficient for TC CCTs (0.47) is much lower than that for non-TC land and ocean CCTs (0.79 and 0.84, respectively). The main reason is that all TC CCTs have the maximum $Z_{20\mathrm{dB}Z}$ greater than 7 km and most of them have the minimum T_{B11} colder than 220 K, while non-TC CCTs have a much wider range of these two parameters.

c. *Selection of overshooting properties and convective parameters*

As mentioned previously, although DCUs are not referred to as overshooting convection, the word overshooting is used to define overshooting properties for both DCUs and CCTs. By following Liu and Zipser (2005), four overshooting properties, including overshooting distance, area, volume, and precipitating ice mass, are estimated as follows: For each DCU, the overshooting distance is how high the maximum 20-dBZ echo height exceeds 14 km. The overshooting area of each DCU is calculated by multiplying the number of PR pixels with 14-km reflectivity greater than 20 dBZ by the size of each pixel (~17.92 km^2 before the TRMM boost and ~20.35 km^2 after the boost). The overshooting volume of each DCU is calculated by summing all pixels above 14 km with reflectivity >20 dBZ and multiplying the unit volume of each pixel (~4.48 km^3 before the TRMM boost and ~5.09 km^3 after the boost). The overshooting precipitating ice mass is calculated by integrating the precipitating ice mass of PR pixels above 14 km. The precipitating ice mass of each PR pixel is obtained using the same radar reflectivity–ice mass

TABLE 1. Population and characteristics of very deep convection (VDC) defined by PR maximum $Z_{20dBZ} \geq 14$ km (DCUs) and IR minimum T_{B11} colder than tropopause temperature (CCTs) for TC and non-TC over land and ocean categories.

			Non-TCPFs					
	TCPFs		Land		Ocean		Total	
Population (No.)	17 088		274 729		539 760		814 489	
Contribution to total PFs (%)	2.1		33.0		64.9		97.9	
Total raining area (10^5 km^2)	2484		20 024		55 858		75 882	
Contribution to total raining area (%)	3.2		25.6		71.3		96.8	
VDC	DCUs	CCTs	DCUs	CCTs	DCUs	CCTs	DCUs	CCTs
Population (No.)	3323	5908	72 333	66 840	61 677	100 234	134 010	167 074
Total overshooting area (10^5 km^2)	9	211	156	505	76	873	232	1378
Fraction of total DCUs or CCTs that are associated with TCs or non-TCs (%)	2.4	3.4	52.7	38.6	44.9	58.0	97.6	96.6
Fraction of total overshooting area that is from TCs, or non-TCPFs (%)	3.8	13.3	64.7	31.8	31.5	54.9	96.2	86.7
Percentage of TCPFs and non-TCPFs that are VDC (%)	19.5	34.6	26.3	24.3	11.4	18.6	16.5	20.5
Total overshooting area divided by total raining area (%)	0.4	8.5	0.8	2.5	0.1	1.6	0.3	1.8
Mean raining area (km^2)	18 716	18 187	7899	10 324	14 557	17 877	10 963	14 856
Mean overshooting area (km^2)	275	3622	216	761	123	871	174	824
Mean overshooting area/mean raining area (%)	1.5	19.9	2.7	7.3	0.8	4.9	1.6	5.5

relation described by Carey and Rutledge (2000). For CCTs, only overshooting distance and area are estimated. The overshooting distance of each CCT is estimated as the temperature difference between the cloud-top T_{B11} and the tropopause temperature T_{trop}: that is, $T_{trop} - T_{B11}$. The overshooting area of each CCT is calculated by multiplying the number of PR pixels with T_{B11} colder than T_{trop} by the size of each pixel (same as the above).

Since the TRMM satellite cannot directly provide information on vertical motions, six convective parameters are selected as proxies of convective intensity for very deep convection in TCs and non-TCs over land and ocean. These include the maximum Z_{20dBZ}, Z_{30dBZ}, and Z_{40dBZ} from the PR, minimum T_{B11} from VIRS and minimum 85- and 37-GHz PCT from the TMI. The maximum Z_{20dBZ}, Z_{30dBZ}, and Z_{40dBZ} are indicators of storm heights and maximum Z_{30dBZ} and Z_{40dBZ} are arguably related to the strength of low to midlevel updrafts. Heymsfield et al. (2010) showed a relationship between the height of the 40-dBZ (30 dBZ) reflectivity and maximum vertical velocity, with a correlation coefficient of 0.6 (0.5). The minimum T_{B11} indicates the cold cloud-top height that a convective cloud reaches, which is always higher than the maximum Z_{20dBZ}. This parameter is associated with both the convective intensity and the level of neutral buoyancy or tropopause height (Liu et al. 2007). The microwave brightness temperatures at 85 and 37 GHz respond to scattering of upwelling radiation by precipitation-sized ice particles, which reduce the observed brightness temperature. To remove the ambiguity that the low brightness temperature attributable to ice scattering could be confused with the cold sea surface temperature, the PCT at 85 (Spencer et al. 1989) and 37 GHz (Cecil et al. 2002) is defined so that PCTs are cold for ice scattering and warm for the sea surface. Both 85- and 37-GHz PCTs are inversely related to the vertically integrated ice water path above the freezing level. The 85-GHz channel responds to both small and large precipitation-sized ice particles, while the 37-GHz channel is influenced more by larger precipitation-sized particles (Cecil et al. 2002).

3. Contribution of TCs to global very deep convection in the tropics (36°S–36°N)

Table 1 summarizes the population and characteristics of TCPFs and non-TCPFs, and very deep convection (DCUs and CCTs) in TCs and non-TCs. It is seen that in general, TCs contribute only 2.1% of total convective precipitation features with size $\geq$1000 km^2. The rest (97.9%) are non-TCPFs with 33% over land and 64.9% over ocean. This study is feature based, similar to Liu and Zipser (2005). To compare with pixel/area-based studies such as Alcala and Dessler (2002), Cairo et al. (2008), and Romps and Kuang (2009), area-based percentages are also calculated in Table 1. The fraction of total surface raining area of PFs that are associated with TCs is 3.2%, only slightly higher than that of the feature-based fraction. As for the population of DCUs and CCTs, it is seen that the number of DCUs is about 1.5 times less than that of CCTs for both TC and non-TC

over ocean categories, while the number of land DCUs is slightly more than that of land CCTs. Only 2.4% (3.4%) of total DCUs (CCTs) are from TCs, while 52.7% (44.9%) are from non-TCs over land and 38.6% (57.9%) are from non-TCs over ocean. The population of very deep convection over land is higher over ocean when using the PR-based definition, while the reverse is true when using the IR-based definition. This is consistent with Liu and Zipser (2005)'s results, which showed that over land systems produce more very deep convection with PR 20-dBZ echo penetrating 14 km. This also indicates that oceanic systems tend to produce more small ice particles around the cloud-top layer that are not detectable by the PR. For the contribution of TCs, 2.4%–3.4% contribution to very deep convection is not much higher than the 2.1% contribution of TCs to the total PFs. This seems to be consistent with previous TRMM PR–based studies that suggested that TC is not a preferred pathway for TTL-penetrating convection (Alcala and Dessler 2002; Cairo et al. 2008; Liu and Zipser 2005; Tao and Jiang 2013) but contradictory to Romps and Kuang (2009)'s results, which suggested that TCs contribute a disproportionately large amount of convection that reaches the stratosphere. Keep in mind, however, that the fraction of overshooting convection in Romps and Kuang (2009) was pixel/area based and based on IR data only. From row 13 of Table 1, the fraction of total overshooting area of CCTs that is from TCs is 13.3%, while the fraction of total raining area of PFs that is from TCs is only 3.2%. In another words, TCs account for only 3.2% of the convective precipitating area in the tropics (36°S–36°N), but they contribute 13.3% of overshooting convection. This result is very similar to Romps and Kuang (2009), who showed that TCs account for 7% of the deep convection in the tropics (30°S–30°N) but 15% of the overshooting convection. It is interesting to notice that this increased contribution of TCs is only seen from the IR-based CCTs but is not obvious in PR-based DCUs. This indicates that TCs only contribute disproportionately large amount of very deep convection containing mainly small ice particles that are not detected by the PR.

Similar results are seen when looking at the percentage of TCPFs and non-TCs that are DCUs or CCTs. From row 10 of Table 1, the feature-based percentage of TCPFs that are DCUs is 19.5%, which is lower than that of non-TCPFs over land (26.3%) and only slightly higher than that of all non-TCPFs (16.5%) and non-TCPFs over ocean (11.4%). However, the percentage of TCPFs that are CCTs (34.6%) is much higher than that of all non-TCPFs (20.5%) and non-TCPFs over land (24.3%) and over ocean (18.6%). For the area-based percentages (11th row of Table 1), a similar trend is seen, but the differences are larger. Overall, non-TCPFs over land have the greatest chance to have 20-dBZ radar echoes penetrating 14 km (0.8%), while TCPFs have the highest percentage with minimum T_{B11} colder than T_{trop} (8.5%). As for the size of DCUs and CCTs, it is found that the mean surface raining area (12th row of Table 1) of TC DCUs is a little larger than that of ocean DCUs but about a factor of 2 larger than that of land DCUs. The mean surface raining area of land CCTs is also much smaller than those of TC and ocean CCTs. TCs have the largest mean overshooting area (13th row of Table 1) for both DCUs and CCTs. The mean overshooting area of TC CCTs is about a factor of 4 larger than that of non-TC CCTs. For non-TC cases, overland DCUs have larger mean overshooting areas and overland CCT have small mean overshooting areas versus those over the ocean. As for the fractional overshooting area defined by mean overshooting area divided by the mean raining area (last row of Table 1), TC DCUs have slightly smaller (higher) fractional overshooting area than land (ocean) DCUs, but TC CCTs have a factor of 3 (4) higher fractional overshooting area than land (ocean) CCTs.

The geographical distribution of number density of total DCUs, non-TC DCUs, TC DCUs, and the fraction of DCUs associated with TCs are presented in Figs. 3a–d, respectively. To remove the sampling bias, the population of DCUs in each 5° × 5° box is normalized with TRMM product 3A25 total pixel numbers. Consistent with Liu and Zipser (2005), very deep convection is found mainly over the west Pacific, central Africa, South America, the intertropical convergence zone (ITCZ), and the South Pacific convergence zone (SPCZ) (Fig. 3a). The global distribution as well as the locations of high number density are very similar between total DCUs (Fig. 3a) and non-TC DCUs (Fig. 3b), which indicates that the majority of DCUs in the tropics (36°S–36°N) are from non-TCs. The geographical distribution of TC DCUs (Fig. 3c) is very similar to that of total TCPFs (Tao and Jiang 2013, their Fig. 2) and TC rainfall (Jiang and Zipser 2010, their Fig. 5). The highest number density of TC DCUs is seen in the NWP basin over a large area east of the Philippine Islands.

By dividing the number of TC DCUs to total DCUs in each 5° × 5° bin, the geographical distribution of the fraction of TC DCUs is quantified and shown in Fig. 3d. Although 97.6% of DCUs in the tropics (36°S–36°N) are from non-TCs (Table 1), there are geographical regions where TCs do contribute a disproportionately large fraction of total DCUs. It is found that TCs contribute about 35% to total DCUs in a region south of the Baja California coast (15°–25°N, 105°–125°W) in the EPA basin, with a maximum fraction of DCUs associated

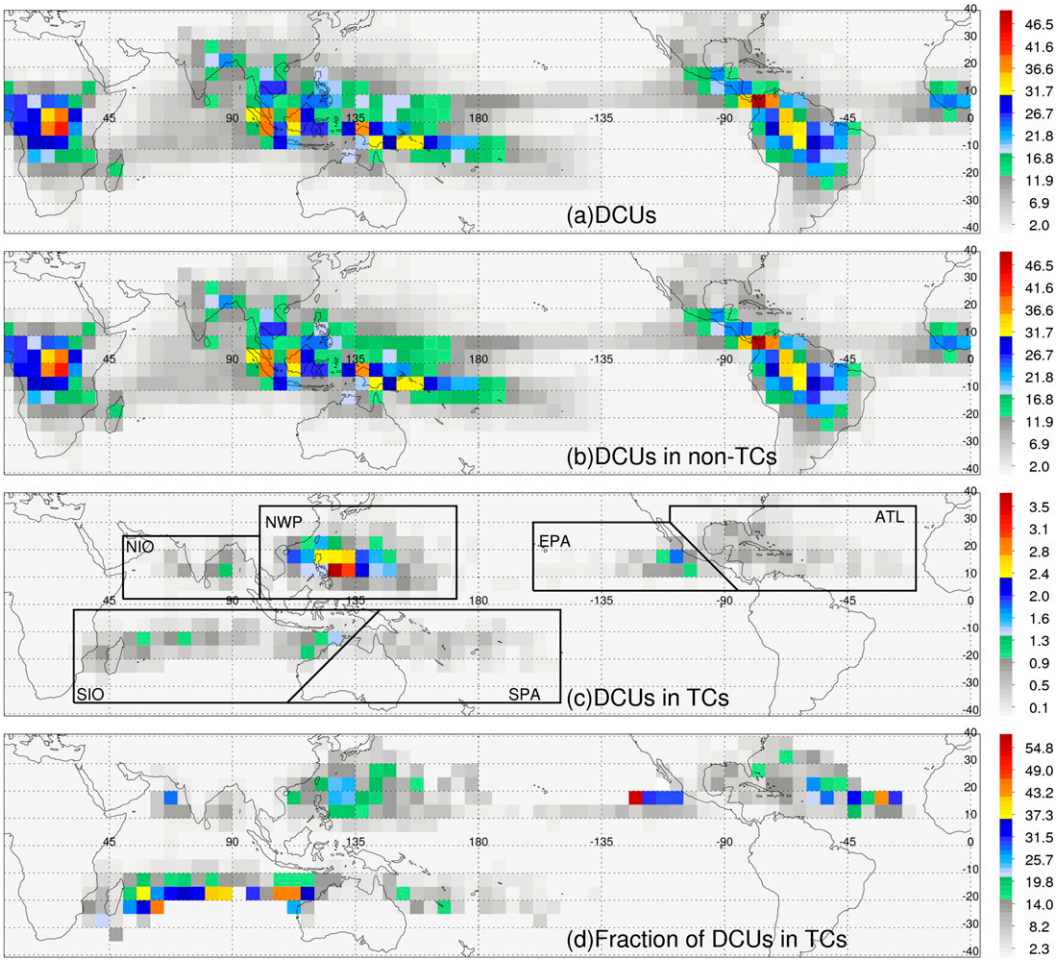

FIG. 3. Global distributions of number density (ppm) of (a) total DCUs (number), (b) DCUs in non-TCs (number), (c) DCUs in TCs (number), and (d) fraction of DCUs in TCs (%). Number density is defined as total number of DCUs in each 5° × 5° bin divided by TRMM 3A25 total pixel numbers to remove sampling bias. Borders of six basins (ATL, EPA, NWP, NIO, SIO, and SPA) are indicated.

with TCs exceeding 55%. Over large areas (between 15° and 20°S) to the east of Madagascar and northwest coast of Australia in the SIO basin, about 33% of DCUs are from TCs. In the northwest ATL basin (15°–20°N, 25°–60°W), approximately 26% of DCUs are from TCs. Moreover, a higher fraction of TC DCUs (about 22%) is detected in a region around the island of Taiwan and northeast of the Philippine Islands (15°–25°N, 120°–135°W). In general, the pattern of fraction of DCUs that are from TCs is similar to the percentage of total rainfall contributed by TCs as shown in Jiang and Zipser (2010).

For comparison, Fig. 4 shows the geographical distributions of number density of total CCTs, non-TC CCTs, and TC CCTs and the fraction of TC CCTs. The general pattern of the number density of total DCUs (Fig. 3a) and total CCTs (Fig. 4a) are quite similar in most regions, except that in the north ATL, to the west of Singapore, and south of Sri Lanka in the Indian Ocean the number density of CCTs is greater than that of DCUs and in central Africa and Madagascar the number density of DCUs is larger than that of CCTs. Consistent with the results of DCUs, the geographical distribution of number density of total CCTs (Fig. 4a) and non-TC CCTs (Fig. 4b) are very similar, indicating that the majority (96.6%, as seen in Table 1) of very deep convection with T_{B11} lower than the T_{trop} are from non-TCs. Moreover, similar patterns are found between TC DCUs (Fig. 3c) and TC CCTs (Fig. 4c).

As seen from Table 1, very deep convection defined with IR (CCTs) has higher fraction attributable to TCs than that for very deep convection defined with PR (DCUs). However, the geographical distribution of the fraction of TC DCUs (Fig. 3d) and that of the fraction of TC CCTs (Fig. 4d) show very similar patterns. The maximum percentage of TC DCUs is in the same region as the maximum percentage of TC CCTs. TCs account

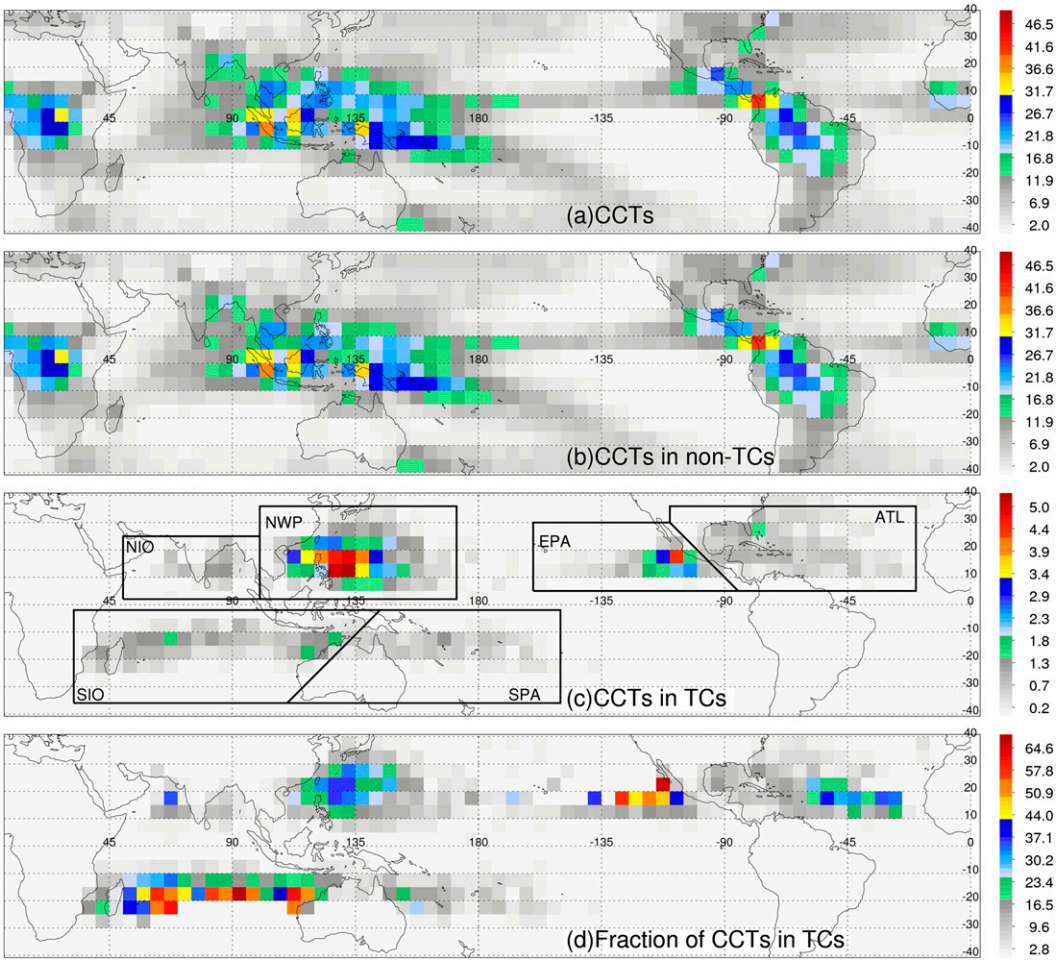

FIG. 4. As in Fig. 3, but for CCTs.

for the majority of convection in the trade wind regions. The contribution of TCs to total CCTs is approximately 43% to the west of the Baja California coast (15°–25°N, 105°–145°W) in the EPA basin, which is 8% higher than the contribution of TCs to total DCUs. Over the east of Madagascar and the northwest coast of Australia in the SIO basin (10°–25°S, 50°–125°E), over the northwest ATL basin (between 15° and 25°N), and around the island of Taiwan and northeast of the Philippine Islands in the NWP basin (15°–25°S, 110°–150°E), about 35%, 27%, and 24% of total CCTs are from TCs, respectively.

To further study the contributions of TCs to total DCUs and CCTs in six TC-prone basins, Table 2 displays the population of total DCUs (CCTs), TC DCUs (CCTs), and the basinwide mean feature- and area-based fractions of DCUs (CCTs) that are from TCs for each basin. No matter which definition is used to define very deep convection (either DCUs or CCTs), the NWP basin always contains the highest population of total very deep convection and TC very deep convection. The greatest fraction, both feature based and area based (6.1% and 11.4%, respectively), of DCUs associated with TCs is observed in NWP basin. The greatest area-based fraction of CCTs associated with TCs is also found in the NWP basin (44.8%), while the greatest feature-based fraction of CCTs associated with TCs is detected in EPA basin (9.9%). The SPA basin has the lowest fraction of CCTs that are from TCs, and the lowest (second lowest) feature-based (area-based) fraction of DCUs that are from TCs. The NIO basin has the lowest area-based fraction of DCUs that are from TCs.

By lowering the threshold temperature for defining very cold cloud, Romps and Kuang (2009) found that TCs' contribution to very deep convection increases disproportionally as the temperature threshold decreases (increasingly colder than the tropopause temperature). A similar result is found in this study. Table 3 shows the feature-based and area-based fractions of DCUs with maximum $Z_{20\mathrm{dB}Z} \geq 14$–18 km that are from TCs and non-TCs over land and ocean. It is obvious that,

TABLE 2. The population of very deep convection (number), very deep convection in TCs (number), and the feature-based and area-based fraction of very deep convection associated with TCs (%) in six TC-prone basins.

	DCUs (max $Z_{20dBZ} \geq 14$ km)				CCTs (min $T_{B11} \leq T_{trop}$)			
Basins	Total No.	No. of TC DCUs	Fraction of DCUs associated with TCs	Fraction of overshooting area contributed by TCs	Total No.	No. of TC DCUs	Fraction of DCUs associated with TCs	Fraction of overshooting area contributed by TCs
ATL	14 655	521	3.6	4.5	25 176	1064	4.2	20.1
EPA	5573	296	5.3	8.6	7181	708	9.9	40.3
NWP	21 518	1319	6.1	11.4	27 042	2404	8.9	44.8
NIO	8254	213	2.6	3.9	8293	265	3.2	23.7
SIO	15 219	682	4.5	8.9	16 730	988	5.9	28.0
SPA	15 655	292	1.9	4.1	21 624	479	2.2	12.2

as the height threshold increases from 14 to 18 km, the feature- (area) based fraction of DCUs contributed by TCs increases from 2.4% (3.8%) to 5.2% (5.7%), while the fractional DCUs from over land non-TCs increases from 52.7% (64.7%) to 85.5% (85.7%) and the fractional DCUs from over ocean non-TCs decreases dramatically from 44.9% (31.5%) to 9.3% (8.6%). Table 4 shows the feature-based and area-based fractions of CCTs with $T_{trop} - T_{B11} \geq 0$–10 K that are from TCs and non-TCs over land and ocean. Similar to Table 3 for DCUs, as the temperature threshold decreases from 0 to 10 K colder than the tropopause, the feature- (area) based fraction of CCTs contributed by TCs increases from 3.4% (13.3%) to 5.0% (17.9%), while the fractional CCTs from over land non-TCs increases from 38.7% (31.8%) to 50.7% (61.2%) and the fractional CCTs from over ocean non-TCs decreases from 57.9% (54.9%) to 44.3% (20.9%).

4. Comparison of the overshooting and convective properties in very deep convection in TCs and non-TCs

a. Overshooting properties

In sections 4a and 4b(1), the overshooting and convective properties will be compared between TC and non-TC DCUs/CCTs. Previous studies have found that the convective intensity in different TC regions is different. Szoke et al. (1986) found that the mean radar reflectivity profiles are similar above the freezing level for convective cells in hurricane rainbands and in general tropical oceanic rainfall systems, but the mean eyewall reflectivity profile above the freezing level shows stronger convective intensity. Jorgensen and LeMone (1989) and Black et al. (1996) found that inner rainbands exhibit weaker updraft magnitudes than do eyewalls. Cecil et al. (2002) and Cecil and Zipser (2002) showed that the convective cores within the eyewall region have the highest reflectivity compared with those in the inner and outer rainbands. Therefore, here TC DCUs and CCTs will be further separated into IC, IB, and OB DCUs and CCTs. The IC region includes complete eyewalls, incomplete or partial eyewalls, concentric eyewalls, and near-center convection for storms without an eye. The IB region includes banded or bloblike precipitation immediately outside of the IC boundary. The OB region includes outward spiraling banded precipitation and any precipitation features associated with the cyclone located beyond about 150–200 km from the storm center. Please refer to section 2a of Jiang et al. (2013) for details of separation of IC, IB, and OB regions. Non-TC DCUs and CCTs will be separated into land and ocean DCUs and CCTs.

Probability density functions (PDFs) of overshooting distance, area, volume and precipitating ice mass for TC DCUs in the IC, IB, and OB region (called IC DCUs, IB DCUs, and OB DCUs, respectively) and non-TC land and ocean DCUs) are shown in Fig. 5. The PDF distribution of overshooting distance for IC DCUs is wider and shifted toward higher values than those for other

TABLE 3. Feature-based and area-based fractions of DCUs that are from TCs and non-TCs over land and ocean according to different maximum 20-dBZ echo height thresholds.

Z_{20dBZ} (km)	≥14	≥15	≥16	≥17	≥18
Feature-based fraction of TC DCUs (%)	2.4	2.8	3.3	3.8	5.2
Feature-based fraction of land DCUs (%)	52.7	58.9	68.0	77.6	85.5
Feature-based fraction of ocean DCUs (%)	44.9	38.3	28.7	18.6	9.3
Area-based fraction of TC DCUs (%)	3.8	3.9	4.3	4.9	5.7
Area-based fraction of land DCUs (%)	64.7	68.1	73.7	79.6	85.7
Area-based fraction of ocean DCUs (%)	31.5	28.0	22.0	15.5	8.6

TABLE 4. Feature-based and area-based fractions of CCTs that are from TCs and non-TCs over land and ocean according to various differences between tropopause temperature and IR brightness temperature.

$T_{trop} - T_{B11}$ (K)	≥0	≥2	≥4	≥6	≥8	≥10
Feature-based fraction of TC CCTs (%)	3.4	3.7	4.1	4.4	4.7	5.0
Feature-based fraction of land CCTs (%)	38.7	40.0	41.9	44.4	47.4	50.7
Feature-based fraction of ocean CCTs (%)	57.9	56.3	54.0	51.2	47.9	44.3
Area-based fraction of TC CCTs (%)	13.3	15.1	16.8	17.9	18.3	17.9
Area-based fraction of land CCTs (%)	31.8	37.1	43.3	49.6	55.6	61.2
Area-based fraction of ocean CCTs (%)	54.9	47.8	39.9	32.5	26.1	20.9

categories (Fig. 5a). From the statistics (including mean, median, standard deviation, mode, and skewness) of overshooting distance, area, volume, and precipitating ice mass shown in Table 5, ocean DCUs have the lowest mean and median values of overshooting distance, while DCUs in the inner core region produce the highest overshooting distance. The distributions of overshooting distance for OB, IB, and land DCUs are similar with same median value. From Table 5, the modes of overshooting area, volume, and precipitating ice mass for IC (and IB for overshooting area only) DCUs are the greatest, followed by those of IB, OB, land, and ocean DCUs. IB DCUs have the highest mean and median values of overshooting area, followed by IC, OB, land, and ocean DCUs in decreasing order. IC DCUs have the highest mean and median values of overshooting volume and precipitating ice mass, followed by IB, OB, land, and ocean DCUs in decreasing order. Overall, TC (including IC, IB, and OB regions) DCUs has slightly higher overshooting distance, area, volume, and ice mass than land DCUs but much higher than ocean DCUs (not shown). The differences of overshooting properties among IC, IB, OB, land, and ocean DCUs as shown in Fig. 5 are statistically significant at the 99% level.

Similarly, PDFs of overshooting distance and area for IC, IB, OB, land, and ocean CCTs are presented in Fig. 6 and the statistics are shown in Table 6. The mode, mean, and median values of overshooting distance for IC CCTs are the highest, followed by that of OB, IB, ocean, and land CCTs in decreasing order. As for overshooting area, the modes for IB and IC CCTs are much larger than those for OB, land, and ocean CCTs (Fig. 6b and Table 6). IB CCTs produce the largest overshooting area, closely followed by IC CCTs. Mean and median values of overshooting area for TC (including IB, IC, and OB) CCTs are about a factor of 4–5 larger than those of land and ocean CCTs. The differences of overshooting properties among IC, IB, OB, land, and ocean CCTs as shown in Fig. 6 are statistically significant at the 99% level.

To summarize Figs. 5 and 6, for very deep convection defined by either PR- (DCUs) or IR- (CCTs) based definition, the TC inner core region has the highest overshooting distance, while the TC inner rainband region has the largest overshooting area. For DCUs, the overshooting characteristics are similar between the non-TC land and TC outer rainband regions. For CCTs, the overshooting area in TCs is much larger than that in non-TCs. In general, the oceanic non-TC systems have the weakest overshooting characteristics.

b. *Convective proxies*

1) COMPARISON BETWEEN TCS AND NON-TCS

Figure 7 shows the PDFs of six selected convective parameters for TC DCUs in the IC, IB, and OB region and non-TC DCUs over land and over ocean. The statistics of these parameters are shown in Table 7. From Fig. 7a and Table 7, IC DCUs have the highest maximum height of 20-dBZ echo, followed by OB and land DCUs, which are closely grouped together. The third

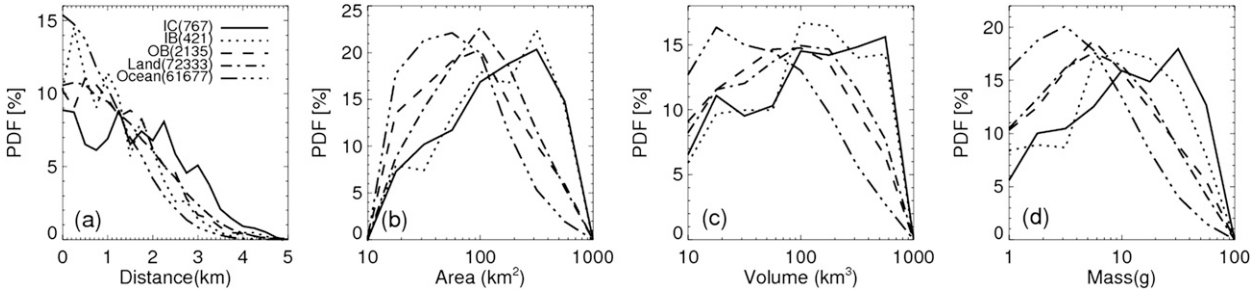

FIG. 5. PDFs of overshooting (a) distance, (b) area, (c) volume, and (d) precipitating ice mass for IC, IB, OB, land, and ocean DCUs. Numbers in parentheses in (a) indicate the sample size.

TABLE 5. The mean, median, standard deviation (STD), mode, and skewness for each parameter shown in Fig. 5.

DCUs	Category	Mean	Median	STD	Mode	Skewness
Distance (km)	IC	1.60	1.5	1.10	0 and 1.25	0.34
	IB	1.14	1.0	0.92	0.25	1.02
	OB	1.25	1.0	0.92	0.50	0.66
	Land	1.26	1.0	0.97	0.25	0.72
	Ocean	0.92	0.75	0.78	0	0.93
Area (km^2)	IC	359	204	428	316	3.15
	IB	411	244	514	316	2.96
	OB	218	102	346	100	5.26
	Land	216	122	302	100	6.17
	Ocean	124	72	171	56	5.78
Volume (km^3)	IC	530	214	815	562	3.69
	IB	471	188	839	100	4.76
	OB	284	94	617	100	7.15
	Land	277	107	521	100	7.25
	Ocean	130	51	259	18	7.78
Mass (g)	IC	35.0	17.3	48.0	31.6	3.23
	IB	30.0	14.9	46.3	10.0	4.12
	OB	18.1	6.9	34.6	5.6	6.32
	Land	15.8	6.7	28.1	5.6	7.13
	Ocean	8.6	3.8	15.3	3.2	6.74

highest maximum Z_{20dBZ} is found in IB DCUs, while ocean DCUs have the lowest maximum Z_{20dBZ}. The mode of maximum Z_{30dBZ} for land DCUs is 13 km, which is much higher than those for other categories (Fig. 7b and Table 7). The same is true for the mean and median values of maximum Z_{30dBZ}. IC, OB, and ocean DCUs have similar maximum Z_{30dBZ} mean and median values, which are smaller than those of land DCUs. IB DCUs have the lowest maximum Z_{30dBZ}. Figure 7c shows that the distributions of maximum Z_{40dBZ} are narrower than those of maximum Z_{30dBZ}. Land DCUs have the highest mode value of 6.5 km, while the modes of other categories are only 5 km. The greatest mean and median maximum Z_{40dBZ} values are found in land DCUs, followed by IC, OB, ocean, and IB DCUs (Table 7).

TC DCUs are skewed toward lower minimum T_{B11} than non-TC DCUs (Fig. 7d). IC DCUs have the lowest mean and median values of minimum T_{B11}, followed by IB, OB, ocean, and land DCUs in increasing order (Table 7). The minimum 85-GHz PCT of land DCUs peaks at 130 K, while that of IC DCUs has a double peak, one at 150 K (which is the mode) and the other at 90 K (Fig. 7e). A single 140-K mode value is found all other DCU groups. From Table 7, land DCUs have the smallest mean and median values of minimum 85-GHz PCT, followed by IC, OB, IB, and ocean DCUs, although the differences are very small. The PDFs of minimum 37-GHz PCT for land and IC DCUs skewed to lower values than other DCU categories (Fig. 7f). Land DCUs have the lowest mean and median values of

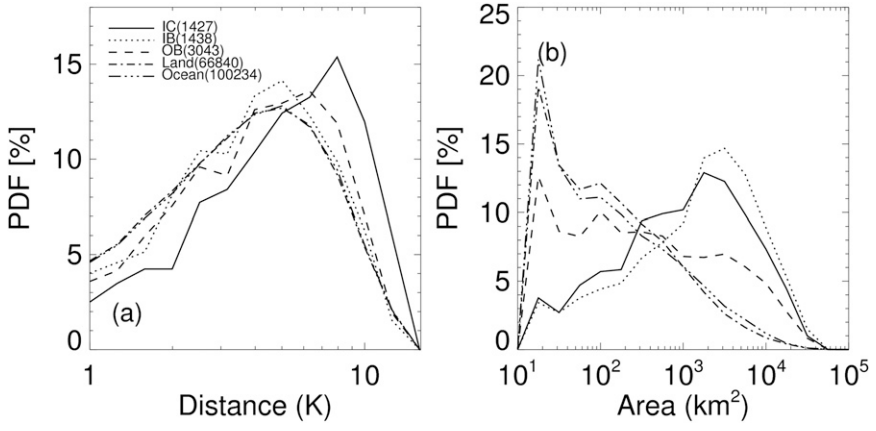

FIG. 6. PDFs of overshooting (a) distance and (b) area for IC, IB, OB, land, and ocean CCTs. Numbers in parentheses in (a) indicate the sample size.

TABLE 6. The mean, median, standard deviation, mode, and skewness for each parameter shown in Fig. 6.

CCTs	Category	Mean	Median	STD	Mode	Skewness
Distance (km)	IC	5.96	5.47	3.73	7.94	0.38
	IB	4.46	3.95	3.16	5.01	0.73
	OB	4.71	4.14	3.30	6.31	0.64
	Land	4.22	3.55	3.20	5.01	0.87
	Ocean	4.26	3.58	3.21	5.01	0.86
Area (km^2)	IC	4176	1506	6525	1778	2.74
	IB	4997	2340	7098	3162	2.53
	OB	2612	305	5694	18	3.65
	Land	755	102	2540	18	9.74
	Ocean	871	90	2872	18	10.00

minimum 37-GHz PCT, followed by IC, IB, OB, and ocean DCUs in increasing order (Table 7). Significance tests show that the differences among different DCU categories for each convective parameter are statistically significant at the 99% level.

For comparison, PDFs of the six selected convective parameters for CCTs are shown in Fig. 8. Different from DCUs, broader distributions of the maximum Z_{20dBZ} are found for CCTs (Fig. 8a). IB CCTs are skewed toward lower maximum Z_{20dBZ}, while land, IC, OB, and ocean CCTs are skewed toward higher values. The mode of maximum Z_{20dBZ} is the highest for land CCTs and the lowest for IB CCTs. The mean and median values of maximum Z_{20dBZ} are the highest for land CCTs, followed by OB, IC, ocean, and IB CCTs in decreasing order (Table 8). This is different from DCUs in which IC DCUs have the highest maximum Z_{20dBZ}. Similar patterns are found for the maximum Z_{30dBZ} (Fig. 8b) and Z_{40dBZ} (Fig. 8c), in which land CCTs are skewed toward higher values, while IB, IC, OB, and ocean CCTs are skewed toward lower values. Also, the PDFs for IC, OB, and ocean CCTs are closely grouped together. For the maximum Z_{30dBZ} and Z_{40dBZ}, the mean and median values are the highest for land CCTs, followed by OB, IC, ocean, and IB CCTs in decreasing order (Table 8). Same as DCUs, TC CCTs are also skewed slightly toward lower minimum T_{B11} compared with land and ocean CCTs in non-TCs (Fig. 8d). Smaller differences of the minimum T_{B11} in TCs and non-TCs are found for CCTs compared with DCUs. IC CCTs

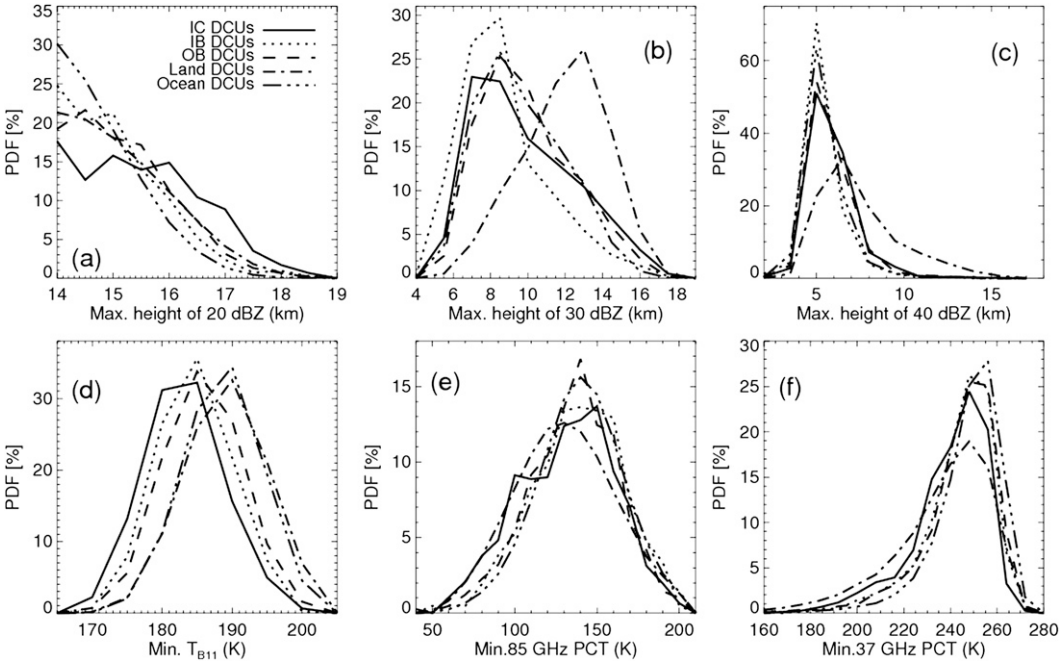

FIG. 7. PDFs of (a) maximum Z_{20dBZ}, (b) maximum Z_{30dBZ}, (c) maximum Z_{40dBZ}, (d) minimum T_{B11}, (e) minimum 85-GHz PCT, and (f) minimum 37-GHz PCT for IC, IB, OB, land, and ocean DCUs.

TABLE 7. The mean, median, standard deviation, mode, and skewness for each parameter shown in Fig. 7.

DCUs	Category	Mean	Median	STD	Mode	Skewness
Max height of 20 dBZ (km)	IC	15.60	15.50	1.10	14.00	0.34
	IB	15.14	15.00	0.92	14.00	1.02
	OB	15.25	15.00	0.92	14.50	0.66
	Land	15.26	15.00	0.97	14.00	0.72
	Ocean	14.92	14.75	0.78	14.00	0.93
Max height of 30 dBZ (km)	IC	10.46	10.00	2.72	7.00	0.56
	IB	9.40	9.00	2.37	8.50	0.96
	OB	10.56	10.25	2.42	8.50	0.54
	Land	12.57	12.75	2.28	13.00	−0.30
	Ocean	10.27	10.00	2.29	8.50	0.44
Max height of 40 dBZ (km)	IC	6.52	6.25	1.32	5.00	1.76
	IB	5.94	5.75	1.18	5.00	0.71
	OB	6.44	6.25	1.28	5.00	1.73
	Land	8.10	7.50	2.32	6.50	1.04
	Ocean	6.12	6.00	1.23	5.00	2.00
Min IR (K)	IC	185.7	185.5	5.6	185	0.14
	IB	187.4	187.0	6.0	185	1.97
	OB	188.3	188.2	5.6	185	0.16
	Land	191.7	191.7	6.0	190	0.08
	Ocean	191.1	191.1	5.5	190	0.02
Min 85-GHz PCT (K)	IC	136.4	138.9	29.7	150	−0.23
	IB	143.5	145.5	28.5	140	−0.21
	OB	141.0	142.5	27.1	140	−0.21
	Land	135.9	135.2	30.7	130	0.10
	Ocean	145.1	145.4	26.7	140	−0.07
Min 37-GHz PCT (K)	IC	243.4	246.9	17.2	248	−1.56
	IB	247.1	250.9	16.6	248	−2.01
	OB	248.0	251.4	16.0	248	−1.70
	Land	240.0	244.6	22.0	248	−1.32
	Ocean	251.3	254.2	15.2	256	−2.00

have the coldest minimum T_{B11} mean and median values in general, followed by OB, IB, land, and ocean CCTs in increasing order (Table 8). As for the minimum 85- and 37-GHz PCT, the lowest mean and median values are found in land CCTs, while the highest are found in IB CCT. Other CCT categories are in between. Similarly, Figs. 8e,f show that land CCTs are skewed toward lower values, while IB CCTs are skewed toward higher values. Significance tests show that the differences among different CCT categories for each convective parameter are statistically significant at the 99% level.

To summarize Figs. 7 and 8, DCUs in the TC inner core region have the highest maximum $Z_{20\text{dB}Z}$, which implies that the IC region produces the height radar echo top statistically. Land DCUs have the highest maximum $Z_{30\text{dB}Z}$ and $Z_{40\text{dB}Z}$, which implies that over land non-TCs produce the strongest low to middle level updrafts. However, the highest maximum $Z_{20\text{dB}Z}$, $Z_{30\text{dB}Z}$, and $Z_{40\text{dB}Z}$ are all found in land CCTs, which may imply that CCTs over land produce the strongest updrafts in all levels. For both DCUs and CCTs, the very deep convection in TCs (especially in the inner core region) have the highest cloud-top height, while very deep convection over land produce the strongest ice-scattering signature as indicated by minimum 85- and 37-GHz PCT. This suggests that deep convection does not necessarily represent intense convection. As concluded by Liu et al. (2007), for the deep cold clouds reaching the same heights, they can be generated from various convective intensities. The result here is consistent with several previous studies. Szoke et al. (1986) found that generally, oceanic convection had lower reflectivity than continental convection. Using high-resolution measurements of vertical velocities in intense convection from the nadir-viewing high-altitude ER-2 Doppler radar (EDOP), Heymsfield et al. (2010) studied the characteristics of different groups of deep convections (i.e., tropical cyclone, oceanic, land, and sea breeze) in the tropics and subtropics. They showed that the tropical cyclone cases had the weakest midlevel updrafts and had peak updrafts at about the 12-km level.

2) COMPARISON OF TC DCUS AND NON-TC DCUS IN SIX SELECTED REGIONS

Liu and Zipser (2005) demonstrated that there are six geographical locations in the tropics having frequent

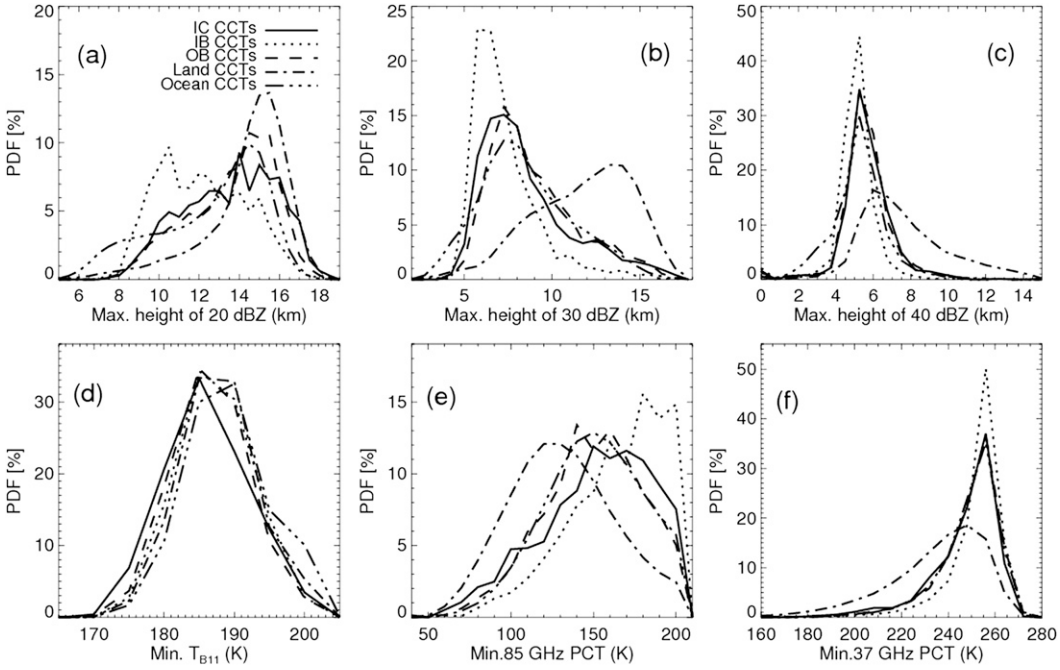

FIG. 8. As in Fig. 7, but for CCTs.

cold IR cloud tops. These locations are over Africa, South America, Indonesia, west Pacific Ocean, east Pacific Ocean, and SPCZ. Figure 9 shows the locations of all DCUs identified in this study. Frequent non-TC DCUs are found in the same regions. Therefore, the six regions outlined with boxes (same regions as in Liu and Zipser 2005) in Fig. 9 are selected to further compare convective properties in non-TC DCUs in these regions with those in TC DCUs over the tropics (36°S–36°N).

The PDFs of the convective parameters for TC DCUs and non-TC DCUs in six selected regions are displayed in Figs. 10a–f. From Fig. 10a, TC DCUs and non-TC DCUs over continental regions (including Africa, South America, and Indonesia) exhibit similar broader maximum $Z_{20\mathrm{dBZ}}$ distributions and are skewed toward higher values compared with non-TC DCUs over oceanic regions (including west Pacific, east Pacific, and SPCZ). The mode of maximum $Z_{20\mathrm{dBZ}}$ is the highest for TC and South America DCUs, which is only 0.25–0.5 km higher than that for other categories (Table 9). The PDF curve of TC DCUs is closely grouped with that of non-TC DCUs over Africa, while the curve of non-TC DCUs over South America is closely grouped with that of non-TC DCUs over Indonesia. Non-TC DCUs in continental regions have broader distributions of the maximum $Z_{30\mathrm{dBZ}}$ (Fig. 10b) and $Z_{40\mathrm{dBZ}}$ (Fig. 10c) that become positively skewed and have higher modes. Non-TC DCUs in Africa have the highest mode values for both maximum $Z_{30\mathrm{dBZ}}$ and $Z_{40\mathrm{dBZ}}$ (Table 9). For the maximum $Z_{30\mathrm{dBZ}}$, the distributions for non-TC DCUs over the west Pacific and east Pacific are similar, while the distributions for TC DCUs and SPCZ DCUs are similar. All oceanic DCUs (including TC DCUs) have smaller mode values of maximum $Z_{30\mathrm{dBZ}}$ and $Z_{40\mathrm{dBZ}}$ than continental DCUs (Table 9). The maximum $Z_{40\mathrm{dBZ}}$ distribution of TC DCUs is similar to that of non-TC DCUs over Indonesia, while the curves for non-TC DCUs over oceanic regions are closely grouped (Fig. 10c). TC DCUs are skewed toward lower minimum T_{B11} compared with all non-TC DCUs, with the coldest mode value (Fig. 10d and Table 9). For the minimum 85-GHz PCT (Fig. 10e) and 37-GHz PCT (Fig. 10f), non-TC DCUs over Africa have the coldest mode values. Non-TC DCUs in continental regions and TC DCUs have broader distributions and are skewed toward lower values compared with non-TC DCUs in oceanic regions. The PDFs of TC DCUs are similar to those of non-TC DCUs in South America, except that DCUs in South America have higher fraction of minimum 37-GHz PCT greater than 250 K.

From Table 9, TC and Africa DCUs have similar and the highest mean and median values of maximum $Z_{20\mathrm{dBZ}}$, followed by the non-TC DCUs over South America, Indonesia, west Pacific, SPCZ, and east Pacific in deceasing order. Non-TC DCUs over Africa have the highest mean and median values of maximum $Z_{30\mathrm{dBZ}}$ as well as $Z_{40\mathrm{dBZ}}$, followed by non-TC DCUs over South America and Indonesia; TC DCUs; and non-TC DCUs

TABLE 8. The mean, median, standard deviation, mode, and skewness for each parameter shown in Fig. 8.

CCTs	Category	Mean	Median	STD	Mode	Skewness
Max height of 20 dBZ (km)	IC	13.67	14.00	2.33	14.00	−0.17
	IB	12.28	12.25	2.23	10.50	0.32
	OB	13.77	14.25	2.15	14.50	−0.45
	Land	14.52	15.00	2.16	15.50	−1.27
	Ocean	12.73	13.50	2.72	14.50	−0.59
Max height of 30 dBZ (km)	IC	8.87	8.00	2.74	7.25	1.19
	IB	7.58	7.00	2.02	5.75	2.05
	OB	9.24	8.50	2.59	7.25	0.95
	Land	11.96	12.25	2.92	13.25	−0.53
	Ocean	8.78	8.50	2.67	7.25	0.52
Max height of 40 dBZ (km)	IC	5.94	5.75	1.68	5.25	1.79
	IB	5.31	5.25	1.41	5.25	2.10
	OB	5.97	5.75	1.38	5.25	2.38
	Land	7.82	7.50	2.65	6.00	0.48
	Ocean	5.50	5.50	1.63	5.25	1.03
Min IR (K)	IC	188.8	188.5	6.4	185	0.42
	IB	190.2	189.7	5.9	185	0.62
	OB	189.4	189.1	6.0	185	0.75
	Land	192.6	190.8	8.8	185	1.36
	Ocean	197.6	193.7	12.0	190	0.83
Min 85-GHz PCT (K)	IC	160.5	163.6	35.3	150	−0.43
	IB	176.5	182.0	31.6	180	−0.70
	OB	157.5	157.9	32.0	140	−0.16
	Land	138.4	135.8	33.9	120	0.31
	Ocean	158.8	158.2	32.1	150	−0.07
Min 37-GHz PCT (K)	IC	251.1	255.4	15.1	256	−2.01
	IB	256.0	259.2	11.5	256	−2.74
	OB	252.9	256.4	13.9	256	−1.98
	Land	238.6	243.2	21.4	248	−1.20
	Ocean	252.4	255.9	14.2	256	−2.09

over SPCZ, west Pacific, and east Pacific in deceasing order. The maximum $Z_{30\text{dB}Z}$ and $Z_{40\text{dB}Z}$ of TC DCUs are lower than or similar to those of DCUs in non-TCs over Indonesia but are higher than that in oceanic regions, respectively. The lowest minimum T_{B11} is observed for TC DCUs. Only small differences of the minimum T_{B11} distributions are seen among non-TC DCUs in different selected regions. As for the minimum 85- and 37-GHz PCTs, Africa DCUs have the lowest mean and median values. Comparable minimum 85- and 37-GHz PCTs are detected for TC DCUs and non-TC DCUs over South America, which is lower than those of non-TC DCUs in the other regions. The highest mean and median values of minimum 85- and 37-GHz PCT are seen in west Pacific DCUs. Significance tests show that the differences of each convective parameter among TC DCUs and non-TC DCUs in six selected regions are statistically significant at the 99% level. Similar results were seen when plotting the same figure as Fig. 10 but for CCTs, except that CCTs in the three continental

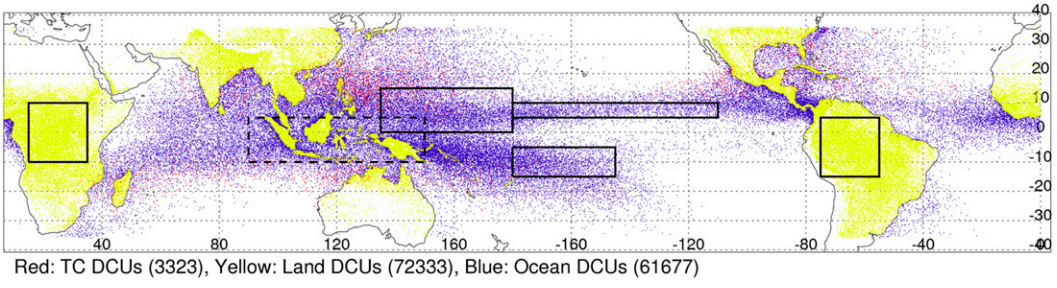

FIG. 9. Locations of DCUs in TCs (red dots), non-TCs over land (yellow), and non-TCs over ocean (blue dots). Also shown are the boundaries of six selected regions with frequent non-TC DCUs, including Africa, Indonesia (the dashed-line box), west Pacific Ocean, east Pacific Ocean, SPCZ, and South America. Numbers in parentheses indicate the total sample size.

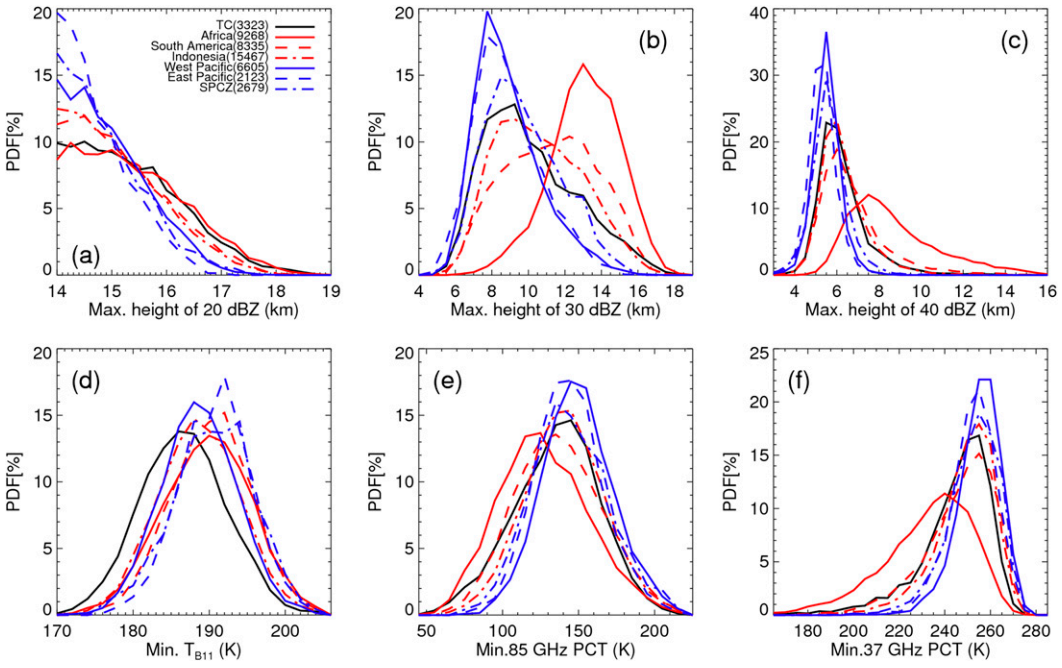

FIG. 10. As in Fig. 7, but for TC DCUs and non-TC DCUs over Africa, South America, Indonesia, west Pacific, east Pacific, and SPCZ. The sample sizes for DCUs in each region are indicated in parentheses in (a).

regions have higher maximum $Z_{20\text{dBZ}}$ than that in TC CCTs, which is higher than that in CCTs in the three oceanic regions.

3) DISCUSSION

Table 5 summarizes the mean characteristics of DCUs and CCTs in TCs and non-TCs over land and over ocean. The areas of 20-, 30-, 40-dBZ echo reaching different height levels are derived from the TRMM PR observations, as well as the mean 20-, 30-, and 40-dBZ echo height and the area of PR 2A25 rain. The IR cloud-top height is calculated from the minimum T_{B11} using the ERA-Interim temperature profile. The tropopause height and temperature, vertical wind shear, total precipitable water (TPW), and convective available potential energy (CAPE) are derived from the ERA-Interim. The vertical wind shear is defined as the difference between the horizontal wind fields at the 200- and 850-hPa levels. The CAPE calculated here is the pseudoadiabatic CAPE assuming total fallout (all condensates are removed from the parcel immediately upon formation; Molinari et al. 2012). Because of the coarse resolution (1.5° × 1.5°) of the ERA-Interim data and the small size of very deep convection, it is assumed that the ERA-Interim-derived parameters interpolated to the location and time of each precipitating and convective feature represent the environmental factors of the very deep convection.

Based on the mean statistics given in Table 10, the schematic of the structure of "typical" TC, land, and ocean DCUs and CCTs are constructed in Fig. 11. TC DCUs (Fig. 11a) and CCTs (Fig. 11d) have a much larger surface raining area than ocean DCUs (Fig. 11c) and CCTs (Fig. 11f). Land DCUs (Fig. 11b) and CCTs (Fig. 11e) have the smallest surface raining area. The widths of 20-, 30-, and 40-dBZ echo outlines are based on the mean area reaching different levels listed in Table 10. Areas of 20-dBZ echo reaching 6–14 km are larger for TC DCUs than land DCUs, which are larger than for ocean DCUs. However, this order is only true for area of 20-dBZ echo reaching 6 km for CCTs. At 10 and 14 km, the area is larger for land CCTs than TC CCTs, which is larger than for ocean CCTs. Both land DCUs and CCTs have the largest areas of 30-dBZ echo reaching 6–14 km and 40-dBZ echo reaching 4 km. The mean 20-dBZ heights of TC, land, and ocean DCUs are similar but that of land CCTs is about 1 km higher than that of TC CCTs. As for the mean 30- and 40-dBZ heights, very deep convection over land always have the highest values, about 2–3 km higher than those for TCs and oceanic non-TCs. Comparing DCUs with CCTs, DCUs always produce larger area of 20-, 30- and 40-dBZ echo reaching different heights than their corresponding CCTs. The only exception is that land DCUs have a slightly smaller area of 20-dBZ echo reaching 6 km than that of land CCTs. Furthermore, DCUs usually reach greater mean IR top height and 20-, 30- and 40-dBZ echo top

TABLE 9. The mean, median, standard deviation, mode, and skewness for each parameter shown in Fig. 10.

CCTs	Category	Mean	Median	STD	Mode	Skewness
Max height of 20 dBZ (km)	TC	15.31	15.25	0.98	14.50	0.66
	Africa	15.37	15.25	0.99	14.25	0.57
	South America	15.14	15.00	0.88	14.50	0.71
	Indonesia	15.09	15.00	0.86	14.00	0.78
	West Pacific	14.92	14.75	0.74	14.00	0.73
	East Pacific	14.70	14.5	0.63	14.00	0.88
	SPCZ	14.85	14.75	0.73	14.00	0.92
Max height of 30 dBZ (km)	TC	10.39	10.00	2.51	9.25	0.58
	Africa	13.34	13.50	1.92	13.00	−0.34
	South America	11.48	11.50	2.48	12.25	−0.03
	Indonesia	10.86	10.75	2.33	9.25	0.31
	West Pacific	9.17	8.75	1.83	7.75	0.88
	East Pacific	9.13	9.00	1.84	7.75	0.58
	SPCZ	9.94	9.75	2.06	8.50	0.39
Max height of 40 dBZ (km)	TC	6.39	6.25	1.29	5.50	1.62
	Africa	8.83	8.25	2.18	7.50	1.00
	South America	6.86	6.50	1.63	6.00	1.58
	Indonesia	6.45	6.25	1.19	6.00	1.61
	West Pacific	5.63	5.50	0.68	5.50	−0.43
	East Pacific	5.44	5.50	0.79	5.50	0.17
	SPCZ	5.75	5.75	0.89	5.50	−0.26
Min IR (K)	TC	187.6	187.5	5.8	186	0.40
	Africa	190.7	190.8	5.8	190	−0.09
	South America	191.2	191.3	5.3	192	−0.03
	Indonesia	189.6	189.6	5.4	188	0.09
	West Pacific	189.6	189.5	5.1	188	0.22
	East Pacific	191.2	192.0	4.7	192	−0.07
	SPCZ	191.5	191.7	5.4	194	−0.19
Min 85-GHz PCT (K)	TC	140.3	141.9	28.0	145	−0.23
	Africa	132.1	130.2	29.1	125	0.25
	South America	141.9	140.7	28.3	135	0.13
	Indonesia	145.7	145.6	26.0	145	0.04
	West Pacific	154.4	153.9	23.1	145	0.13
	East Pacific	148.7	148.0	22.4	145	0.17
	SPCZ	149.3	148.1	25.7	135	0.17
Min 37-GHz PCT (K)	TC	246.8	250.4	16.5	255	−1.70
	Africa	234.8	238.0	19.9	240	−0.86
	South America	248.9	251.9	15.7	255	−1.07
	Indonesia	251.0	253.2	13.3	255	−1.20
	West Pacific	257.4	258.4	9.4	255 and 260	−0.85
	East Pacific	254.5	255.5	10.5	255	−1.06
	SPCZ	254.8	256.3	11.6	255	−0.94

heights than corresponding CCTs. This implies that the very deep convection defined by maximum 20-dBZ radar echo reaching 14 km is deeper and more intense than that defined by minimum T_{B11} colder than tropopause temperature. From Table 10, DCUs always have higher mean tropopause height, colder mean tropopause temperature, lower vertical wind shear, higher (or same) TPW, and higher CAPE than those of corresponding CCTs.

Liu and Zipser (2005) compared the overshooting convection over land and ocean and indicated that the convection over land is more intense than that over ocean, with the IR tops closer to the 20-dBZ tops. In Table 10, the mean distance between the IR cloud-top (Z_{IR}) and the 20-dBZ echo top is given for each category. It is found that TC DCUs and CCTs have the largest distance between the IR top and 20-dBZ top, while land DCUs and CCTs have the smallest distance. This again indicates that very deep convection over land is more intense than that in TCs and non-TCs over ocean.

One would expect that environmental conditions, such as vertical wind shear, TPW, CAPE, and entrainment, would play an important role on the structure of very deep convection. Of all these parameters, the vertical wind shear probably exerts the greatest effect on the organization of deep convection (Corbosiero and

TABLE 10. Mean characteristics of DCUs and CCTs in TCs, non-TCs over land, and non-TCs over ocean.

Definition of very deep convection	DCUs			CCTs		
	TC	Land	Ocean	TC	Land	Ocean
Area of 20 dBZ reaching 14 km (km^2)	275	216	124	36	70	17
Area of 20 dBZ reaching 10 km (km^2)	1437	910	731	287	564	251
Area of 20 dBZ reaching 6 km (km^2)	18 893	3737	4672	4982	3968	3706
Area of 30 dBZ reaching 10 km (km^2)	35	435	354	16	113	16
Area of 30 dBZ reaching 6 km (km^2)	363	898	615	209	588	202
Area of 30 dBZ reaching 4 km (km^2)	5255	2194	2944	5227	2081	2186
Area of 40 dBZ reaching 4 km (km^2)	464	728	584	355	411	184
Area of PR 2A25 rain (km^2)	18 716	7899	14 557	18 187	10 324	17 877
Mean min T_{B11} (K)	188	192	191	189	193	198
Mean IR top height (km)	17.1	16.5	16.6	16.8	16.4	15.7
Mean 20-dBZ height (km)	15.3	15.3	14.9	13.4	14.5	12.7
Mean 30-dBZ height (km)	10.4	12.6	10.3	8.7	12.0	8.8
Mean 40-dBZ height (km)	6.4	8.1	6.1	5.8	7.8	5.5
Mean distance $Z_{IR} - Z_{20dBZ}$ (km)	1.8	1.2	1.7	3.4	1.9	3.0
Mean tropopause height (km)	16.04	16.05	16.01	15.89	15.51	14.60
Mean tropopause temperature (K)	193.3	193.2	194.6	194.4	197.3	201.7
Mean vertical wind shear (m s^{-1})	10.7	11.2	10.6	10.9	13.9	15.8
Mean total precipitable water (kg m^{-2})	61	46	56	61	44	48
Mean pseudoadiabatic CAPE (J kg^{-1})	1000	748	564	919	661	351

Molinari 2002; Kaplan et al. 2010; Hence and Houze 2011, 2012a,b; Nguyen and Molinari 2012). Lack of intense updraft storm systems with strong vertical wind shear would be highly titled. Also, updrafts that are titled are more adversely affected by entrainment and therefore difficult for ice particles to penetrate over tropopause. The mean shear value is the highest for ocean CCTs (Table 10), which correspondingly have the lowest IR cloud top and 20-, 30-, and 40-dBZ echo heights. From Table 10, it is seen that very deep convection in TCs usually has smaller shear value than that in non-TCs. This might partially explain why TCs contribute a disproportional amount of very deep convection in the tropics and subtropics. Both TC DCUs and CCTs have much higher mean TPW than non-TC DCUs and CCTs. Very deep convection in TCs has the largest mean value of CAPE, which is 1000 and 919 J kg^{-1} for TC DCUs and CCTs, respectively. Land DCUs and CCTs contain the second greatest values of CAPE, followed by ocean DCUs and CCTs. The value of CAPE decreases dramatically when there is entrainment. Considering that TC DCUs and CCTs have lower vertical wind shear and higher TPW, it is likely that very deep convection in TCs is less tilted as a result of less entrainment and therefore has larger values of CAPE compared with very deep convection in non-TCs. Higher TPW and CAPE can provide more moist convective energy for very deep convection to penetrate tropopause or TTL more easily.

Using the ERA-Interim data, mean skew T–log$p$ diagrams for TC, land, and ocean DCUs and CCTs are displayed in Fig. 12 with the mean values of pseudoadiabatic CAPE, convective inhibition (CIN), lifted condensation level (LCL), and level of neutral buoyancy (LNB) listed. From Fig. 12, it is seen that the shape of CAPE area in very deep convection in TCs is ''skinny'' but extends to higher LNB, while the shape of the CAPE area in very deep convection in over land systems is ''fat'' and ''short.'' This may explain why very deep convection over land is more intense, while very deep convection in TCs overshoots the tropopause more easily.

5. Summary

Based on the 12-yr TRMM tropical cyclone precipitation feature (TCPF) database, both radar and IR observations from TRMM are used to quantify the contribution of TCs to very deep convection in the tropics (36°S–36°N) and to compare TRMM-derived properties of very deep convection in TCs and non-TCs. Two types of very deep convection are defined. The first one is radar based, defined as precipitation features (PFs) with 20-dBZ radar echo penetrating 14 km. This definition is referred to as deep convective updrafts (DCUs). In this study, a PF is defined with TRMM PR near-surface rain rate greater than zero, total PR raining area $\geq$1000 km^2, and minimum 85-GHz PCT $\leq$225 K. The second definition of very deep convection is IR based, defined as PFs with IR cloud-top brightness temperature colder than the tropopause temperature. This definition is referred to as extremely cold cloud

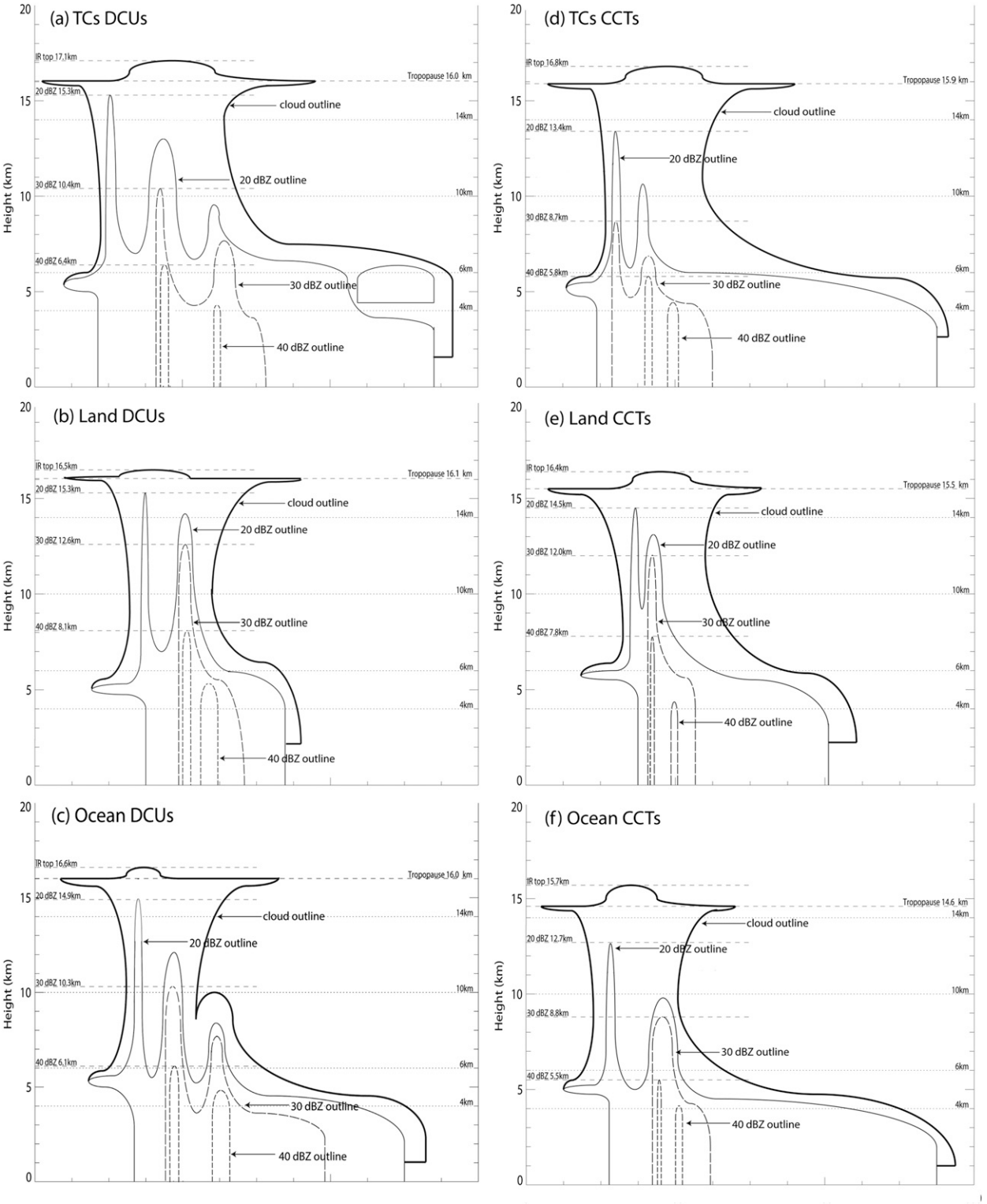

FIG. 11. Schematic of the structure of (a) TC DCUs, (b) land DCUs, (c) ocean DCUs, (d) TC CCTs, (e) land CCTs, and (f) ocean CCTs, demonstrating differences among typical very deep convection systems in TCs and non-TCs over land/ocean. Heights of IR cloud top; tropopause; 20-, 30-, and 40-dBZ echo; and coverage of radar echoes are from Table 10. Please see text for details.

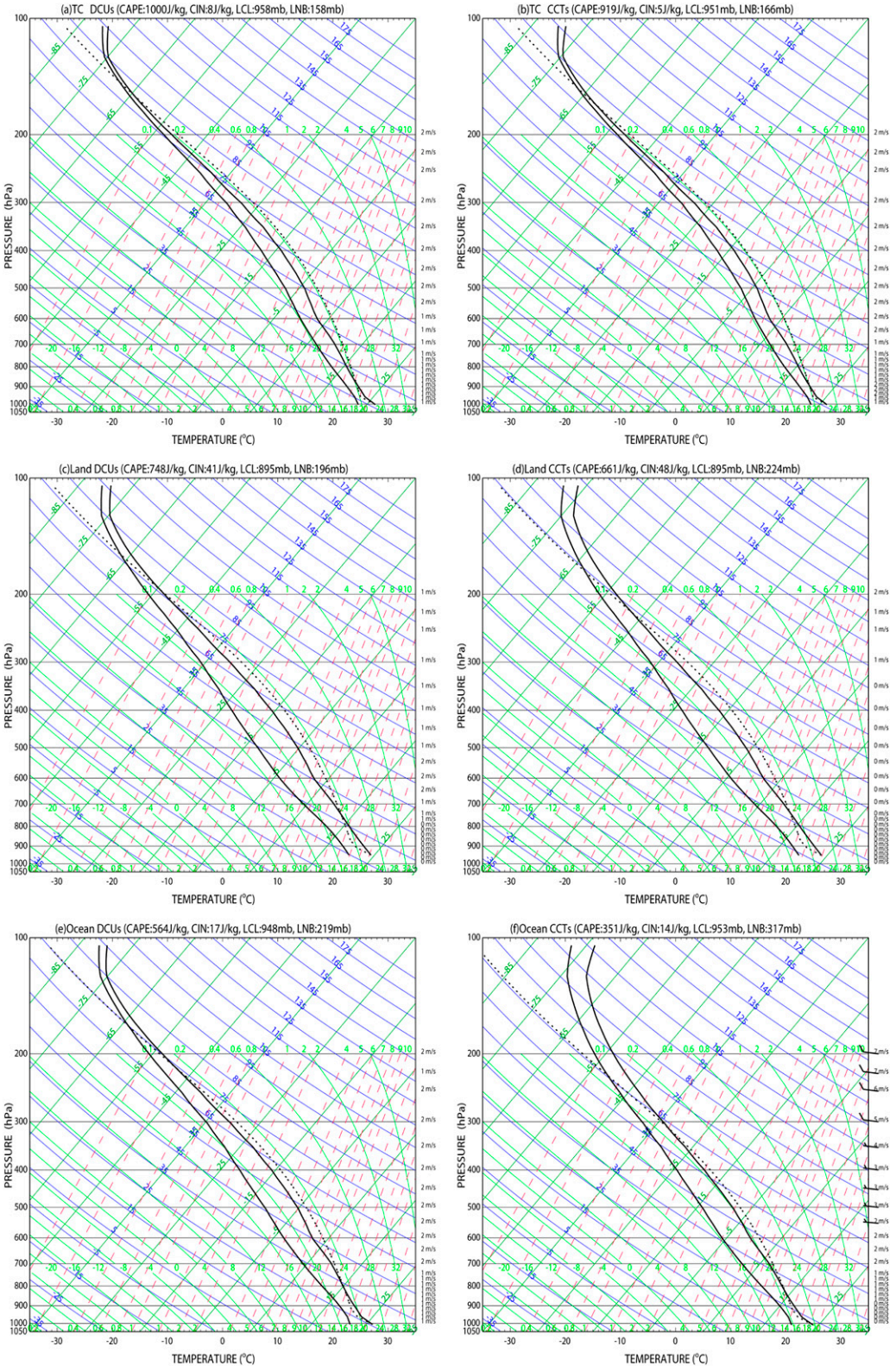

FIG. 12. Mean skew T–log$p$ diagram for (a) TC DCUs, (b) TC CCTs, (c) land DCUs, (d) land CCTs, (e) ocean DCUs, and (f) ocean CCTs. Mean values of CAPE, CIN, LCL, and LNB are listed above each panel.

tops (CCTs). DCUs and CCTs are not the same phenomena, although they have more than 50% overlap. Overall there are more CCTs identified from the 12-yr TRMM data than DCUs. DCUs are deeper and more intense convection than CCTs. For very deep convection in TCs and non-TC over land and ocean categories, TCs and oceanic non-TC systems produce more overshooting cold cloud tops, while land systems produce more very deep convection with radar 20-dBZ echo penetrating 14 km. TC DCUs have slightly smaller (higher) fractional overshooting area than land (ocean) DCUs, but TC CCTs have a factor of 3 (4) higher fractional overshooting area than land (ocean) CCTs.

Based on the feature-based number count, only 2.4% (3.4%) of total DCUs (CCTs) are from TCs, while 52.7% (44.9%) are from non-TCs over land and 38.6% (57.9%) are from non-TCs over ocean. The feature-based 2.4%–3.4% contribution of TCs to total very deep convection in the tropics is not much higher than the 2.1% contribution of TCs to the total PFs. The area-based contribution of TCs to total DCUs in the tropics is 3.8%, which is again not much higher than the 3.2% contribution of TCs to the total raining area of all PFs in the tropics. However, the area-based contribution of TCs to total CCTs is 13.3%, which is much higher than 3.2%. In another words, TCs account for only 3.2% of the convective precipitating area in the tropics (36°S–36°N), but they contribute 13.3% of overshooting convection observed by the IR. Moreover, as the height threshold increases from 14 to 18 km and the temperature threshold decreases from 0 to 10 K colder than the tropopause temperature, both feature- and area-based fraction of very deep convection contributed by TCs increases nearly linearly. This result is very similar to Romps and Kuang (2009), which showed that TCs account for 7% of the deep convection in the tropics (30°S–30°N) but 15% of the overshooting convection. Therefore, this study helps explain the contradictory results between previous TRMM PR–based studies, which suggested that TC is not a preferred pathway for TTL-penetrating convection (Alcala and Dessler 2002; Cairo et al. 2008; Liu and Zipser 2005; Tao and Jiang 2013), and a previous IR-based study by Romps and Kuang (2009), which suggested that TCs contribute a disproportionately large amount of convection that reaches the stratosphere. This study indicates that TCs only contribute disproportionately large amount of very deep convection containing mainly small ice particles that are barely detected by the TRMM PR.

Although the majority (above 96%) of very deep convection in the tropics (36°S–36°N) is from non-TCs (Table 1), there are geographical regions where TCs do contribute a disproportionately large fraction of total very deep convection. These regions include south of the Baja California coast in EPA basin, east of Madagascar and the northwest coast of Australia in the SIO basin, and in the northwest ATL basin, where TCs account for over 25% of very deep convection.

Overshooting properties of very deep convection in the inner core (IC), inner rainband (IB), and outer rainband (OB) regions in TCs and over land and ocean non-TCs are compared. It is shown that IC DCUs have the greatest overshooting distance, volume, and precipitating ice, while IB DCUs have the largest overshooting area. Ocean DCUs have the lowest values of overshooting properties. Land and OB DCUs have similar values of these overshooting properties, while IB DCUs have smaller overshooting distance than land and OB DCUs but higher overshooting area, volume, and ice mass than land and OB DCUs. The distributions of overshooting distance and area for land CCTs are similar to those of ocean CCTs, which both have a little shorter overshooting distance and a factor of 4–5 smaller overshooting area than TC CCTs.

Six convective proxies derived from TRMM including the maximum 20-, 30-, and 40-dBZ echo height ($Z_{20\text{dB}Z}$, $Z_{30\text{dB}Z}$, and $Z_{40\text{dB}Z}$); minimum T_{B11}; and minimum 85- and 37-GHz PCT in very deep convection in TCs and non-TCs are compared. It is found that very deep convection in non-TCs over land has the highest maximum $Z_{30\text{dB}Z}$ and $Z_{40\text{dB}Z}$ and the coldest minimum 85- and 37-GHz PCT, while very deep convection in TCs has the coldest minimum T_{B11}. Oceanic non-TCs have much weaker convective properties in general. Very deep convection in TCs has the largest distance between the IR top height and 20-dBZ top height, while over land non-TCs has the smallest distance. All of these results suggest that convection is much more intense in non-TCs over land but is much deeper or colder in TCs. This may further imply that very deep convection in over-land non-TCs has stronger low- and midlevel updrafts, but very deep convection in TCs has weaker low- and midlevel updrafts and can reach higher IR top height.

Environmental conditions including the vertical wind shear, TPW, and CAPE are estimated from the ERA-Interim data. It is found that very deep convection in TCs usually has smaller shear value than that in non-TCs. Smaller shear may cause the system to be less tilted and therefore less entrainment to be involved. This might partially explain why TCs contribute a disproportional amount of very deep convection in the tropics and subtropics. Very deep convection in TCs has much higher mean TPW and CAPE than that in non-TC DCUs. Higher TPW and CAPE can provide more moist convective energy for very deep convection to

penetrate tropopause or TTL more easily. From the mean skew T–log$p$ diagrams in Fig. 12, the shape of CAPE area in very deep convection in TCs is ''skinny'' and ''tall,'' while the shape of the CAPE area in very deep convection in over land systems is ''fat'' and ''short.'' This may explain why very deep convection over land is more intense, while very deep convection in TCs overshoots the tropopause more easily.

As pointed out by Romps and Kuang (2009), there is the possibility that TCs lift and cool the tropopause more than other mesoscale systems. If this is true, the higher contribution of TCs to extremely cold cloud tops might not imply a higher rate of overshooting. Future research with higher-resolution sounding data in TCs is required to assess whether this effect influences the results.

Acknowledgments. The authors acknowledge Dr. Chuntao Liu for very helpful discussions on the shape of CAPE area in TCs and non-TCs. We thank Drs. Tie Yuan and Chuntao Liu for helping on TRMM data processing. The authors would like to specially thank John Knaff for his tremendous comments and extremely helpful reviews, which lead to significant improvement of the manuscript. We also thank Dr. Ed Zipser and another anonymous reviewer for their helpful comments, which also lead to substantial improvement of the manuscript. The first author received support from NASA New Investigator Program (NIP) award (NNX10AG55G) and the second author received support from NASA Earth and Space Science Fellowship (NESSF) award (NNX11AL66H). Support for this study is also provided by the NASA Precipitation Measurement Mission (PMM) Grant NNX10AE28G and NASA Hurricane Science Research Program (HSRP) Grant NNX10AG34G. The authors thank Drs. Ramesh Kakar and Ming-Ying Wei (NASA headquarters) for their continued support of TRMM/PMM and hurricane science and early career researchers in the field.

APPENDIX

List of Acronyms and Abbreviations

ATL	Atlantic
CAPE	Convective available potential energy
CDFs	Cumulative distribution functions
CIN	Convective inhibition
CCTs	Extremely cold cloud tops
DCUs	Deep convective updrafts
ECMWF	European Centre for Medium-Range Weather Forecasts
EPA	East-central Pacific
IB	Inner rainband
IC	Inner core
IR	Infrared
ITCZ	Intertropical convergence zone
LCL	Lifted condensation level
LNB	Level of neutral buoyancy
JTWC	Joint Typhoon Warning Center
NHC	National Hurricane Center
NIO	North Indian Ocean
NWP	Northwest Pacific
OB	Outer rainband
PCT	Polarization corrected brightness temperature
PDFs	Probability density functions
PF	Precipitation feature
PR	Precipitation radar
SIO	South Indian Ocean
SPA	South Pacific
SPCZ	South Pacific convergence zone
T_{B11}	11-μm brightness temperature
T_{trop}	Tropopause temperature
TC	Tropical cyclone
TCPFs	Precipitation features in tropical cyclones
TRMM	Tropical Rainfall Measuring Mission
VIRS	Visible and Infrared Scanner

REFERENCES

Alcala, C. M., and A. E. Dessler, 2002: Observations of deep convection in the tropics using the Tropical Rainfall Measuring Mission (TRMM) precipitation radar. *J. Geophys. Res.,* **107,** 4792, doi:10.1029/2002JD002457.

Black, M. L., R. W. Burpee, and F. D. Marks Jr., 1996: Vertical motion characteristics of tropical cyclones determined with airborne Doppler radial velocity. *J. Atmos. Sci.,* **53,** 1887–1909, doi:10.1175/1520-0469(1996)053<1887:VMCOTC>2.0.CO;2.

Cairo, F., and Coauthors, 2008: Morphology of the tropopause layer and lower stratosphere above a tropical cyclone: A case study on cyclone Davina (1999). *Atmos. Chem. Phys.,* **8,** 3411–3426, doi:10.5194/acp-8-3411-2008.

Carey, L. D., and S. A. Rutledge, 2000: The relationship between precipitation and lightning in tropical island convection: A C-band polarimetric radar study. *Mon. Wea. Rev.,* **128,** 2687–2710, doi:10.1175/1520-0493(2000)128<2687:TRBPAL>2.0.CO;2.

Cecil, D. J., and E. J. Zipser, 2002: Reflectivity, ice scattering, and lightning characteristics of hurricane eyewalls and rainbands. Part II: Intercomparison of observations. *Mon. Wea. Rev.,* **130,** 785–801, doi:10.1175/1520-0493(2002)130<0785:RISALC>2.0.CO;2.

——, ——, and S. W. Nesbitt, 2002: Reflectivity, ice scattering, and lightning characteristics of hurricane eyewalls and rainbands. Part I: Quantitative description. *Mon. Wea. Rec.,* **130,** 769–784, doi:10.1175/1520-0493(2002)130<0769:RISALC>2.0.CO;2.

Corbosiero, K. L., and J. Molinari, 2002: The effects of vertical wind shear on the distribution of convection in tropical cyclones. *Mon. Wea. Rev.,* **130,** 2110–2123, doi:10.1175/1520-0493(2002)130<2110:TEOVWS>2.0.CO;2.

Dessler, A. E., 2002: The effect of deep, tropical convection on the tropical tropopause layer. *J. Geophys. Res.,* **107,** 4033, doi:10.1029/2001JD000511.

Ebert, E. E., and G. J. Holland, 1992: Observations of record cold cloud-top temperatures in Tropical Cyclone Hilda (1990). *Mon. Wea.*

Rev., **120,** 2240–2251, doi:10.1175/1520-0493(1992)120<2240:OORCCT>2.0.CO;2.

Frank, W. M., 1976: The structure and energetics of the tropical cyclone. Colorado State University Department of Atmospheric Science Paper 258, 180 pp.

Hence, D. A., and R. A. Houze, 2011: Vertical structure of hurricane eyewalls as seen by the TRMM precipitation radar. *J. Atmos. Sci.,* **68,** 1637–1652, doi:10.1175/2011JAS3578.1.

——, and ——, 2012a: Vertical structure of tropical cyclones with concentric eyewalls as seen by the TRMM precipitation radar. *J. Atmos. Sci.,* **69,** 1021–1036, doi:10.1175/JAS-D-11-0119.1.

——, and ——, 2012b: Vertical structure of tropical cyclone rainbands as seen by the TRMM precipitation radar. *J. Atmos. Sci.,* **69,** 2644–2661, doi:10.1175/JAS-D-11-0323.1.

Heymsfield, G. M., L. Tian, A. J. Heymsfield, L. Li, and S. Guimond, 2010: Characteristics of deep tropical and subtropical convection from nadir-viewing high-altitude airborne Doppler radar. *J. Atmos. Sci.,* **67,** 285–308, doi:10.1175/2009JAS3132.1.

Holton, J. R., P. H. Haynes, M. E. McIntyre, A. R. Douglass, R. B. Rood, and L. Pfister, 1995: Stratosphere-troposphere exchange. *Rev. Geophys.,* **33,** 403–439, doi:10.1029/95RG02097.

Iguchi, T., T. Kozu, R. Meneghini, J. Awaka, and K. I. Okamoto, 2000: Rain-profiling algorithm for the TRMM precipitation radar. *J. Appl. Meteor.,* **39,** 2038–2052, doi:10.1175/1520-0450(2001)040<2038:RPAFTT>2.0.CO;2.

Jarvinen, B. R., C. J. Neumann, and M. A. S. Davis, 1984: A tropical cyclone data tape for the North Atlantic basin, 1886–1983: Contents, limitations, and uses. NOAA Tech. Memo. NWS NHC 22, 24 pp. [Available online at http://www.nhc.noaa.gov/pdf/NWS-NHC-1988-22.pdf.]

Jiang, H., and E. J. Zipser, 2010: Contribution of tropical cyclones to the global precipitation from eight seasons of TRMM data: Regional, seasonal, and interannual variations. *J. Climate,* **23,** 1526–1543, doi:10.1175/2009JCLI3303.1.

——, C. Liu, and E. J. Zipser, 2011: A TRMM-based tropical cyclone cloud and precipitation feature database. *J. Appl. Meteor. Climatol.,* **50,** 1255–1274, doi:10.1175/2011JAMC2662.1.

——, E. M. Ramirez, and D. J. Cecil, 2013: Convective and rainfall properties of tropical cyclone inner cores and rainbands from 11 years of TRMM data. *Mon. Wea. Rev.,* **141,** 431–450, doi:10.1175/MWR-D-11-00360.1.

Jorgensen, D. P., and M. A. LeMone, 1989: Vertical velocity characteristics of oceanic convection. *J. Atmos. Sci.,* **46,** 621–640, doi:10.1175/1520-0469(1989)046<0621:VVCOOC>2.0.CO;2.

Kaplan, J., M. DeMaria, and J. A. Knaff, 2010: A revised tropical cyclone rapid intensification index for the Atlantic and eastern North Pacific basins. *Wea. Forecasting,* **25,** 220–241, doi:10.1175/2009WAF2222280.1.

Kummerow, C., W. Barnes, T. Kozu, J. Shiue, and J. Simpson, 1998: The Tropical Rainfall Measuring Mission (TRMM) sensor package. *J. Atmos. Oceanic Technol.,* **15,** 809–817, doi:10.1175/1520-0426(1998)015<0809:TTRMMT>2.0.CO;2.

Liu, C., and E. J. Zipser, 2005: Global distribution of convection penetrating the tropical tropopause. *J. Geophys. Res.,* **110,** D23104, doi:10.1029/2005JD006063.

——, ——, and S. W. Nesbitt, 2007: Global distribution of tropical deep convection: Different perspectives form TRMM infrared and radar data. *J. Climate,* **20,** 489–503, doi:10.1175/JCLI4023.1.

——, ——, D. J. Cecil, S. W. Nesbitt, and S. Sherwood, 2008: University of Utah TRMM cloud and precipitation feature database. *J. Appl. Meteor. Climatol.,* **47,** 2712–2728, doi:10.1175/2008JAMC1890.1.

Lonfat, M., F. D. Marks, and S. S. Chen, 2004: Precipitation distribution in tropical cyclones using the Tropical Rainfall Measuring Mission (TRMM) Microwave Imager: A global perspective. *Mon. Wea. Rev.,* **132,** 1645–1660, doi:10.1175/1520-0493(2004)132<1645:PDITCU>2.0.CO;2.

Mohr, K. I., and E. J. Zipser, 1996: Mesoscale convective systems defined by their 85-GHz ice scattering signature: Size and intensity comparison over tropical oceans and continents. *Mon. Wea. Rev.,* **124,** 2417–2437, doi:10.1175/1520-0493(1996)124<2417:MCSDBT>2.0.CO;2.

Molinari, J., D. M. Romps, D. Vollaro, and L. Nguyen, 2012: CAPE in tropical cyclones. *J. Atmos. Sci.,* **69,** 2452–2463, doi:10.1175/JAS-D-11-0254.1.

Nesbitt, S. W., E. J. Zipser, and D. J. Cecil, 2000: A census of precipitation features in the tropics using TRMM: Radar, ice scattering, and lightning observations. *J. Climate,* **13,** 4087–4106, doi:10.1175/1520-0442(2000)013<4087:ACOPFI>2.0.CO;2.

Newell, R. E., and S. Gould-Stewart, 1981: A stratospheric fountain? *J. Atmos. Sci.,* **38,** 2789–2796, doi:10.1175/1520-0469(1981)038<2789:ASF>2.0.CO;2.

Nguyen, L. T., and J. Molinari, 2012: Rapid intensification of a sheared, fast-moving hurricane over the Gulf Stream. *Mon. Wea. Rev.,* **140,** 3361–3378, doi:10.1175/MWR-D-11-00293.1.

Riehl, H., and J. S. Malkus, 1958: On the heat balance in the equatorial trough zone. *Geophysica,* **6,** 503–538.

Romps, D. M., and Z. M. Kuang, 2009: Overshooting convection in tropical cyclones. *Geophys. Res. Lett.,* **36,** L09804, doi:10.1029/2009GL037396.

Sherwood, S., and A. Dessler, 2001: A model for transport across the tropical tropopause. *J. Atmos. Sci.,* **58,** 765–779, doi:10.1175/1520-0469(2001)058<0765:AMFTAT>2.0.CO;2.

Simmons, A., S. Uppala, D. Dee, and S. Kobayashi, 2006: ERA-Interim: New ECMWF reanalysis products from 1989 onwards. *ECMWF Newsletter*, No. 110, ECMWF, Reading, United Kingdom, 26–35.

Simpson, J., 1990: Global circulation and tropical cloud activity. *Proc. Int. Symp. on Aqua and Planet,* Tokyo, Japan, Tokai University, 77–90.

Spencer, R. W., H. G. Goodman, and R. E. Hood, 1989: Precipitation retrieval over land and ocean with the SSM/I: Identification and characteristics of the scattering signal. *J. Atmos. Oceanic Technol.,* **6,** 254–273, doi:10.1175/1520-0426(1989)006<0254:PROLAO>2.0.CO;2.

Szoke, E. J., E. J. Zipser, and D. P. Jorgensen, 1986: A radar study of convective cells in mesoscale systems in GATE. Part I: Vertical profile statistics and comparison with hurricanes. *J. Atmos. Sci.,* **43,** 182–198, doi:10.1175/1520-0469(1986)043<0182:ARSOCC>2.0.CO;2.

Tao, C., and H. Jiang, 2013: Global distribution of hot towers in tropical cyclones based on 11-yr TRMM Data. *J. Climate,* **26,** 1371–1386, doi:10.1175/JCLI-D-12-00291.1.